DMD Fast Forward. Published on February 6, 2008 as doi:10.1124/dmd.107.019539

DMD # 19539

CONTRIBUTION OF THE *N*-GLUCURONIDATION PATHWAY TO THE OVERALL *IN VITRO* METABOLIC CLEARANCE OF MIDAZOLAM IN HUMANS

Sylvie KLIEBER, Sébastien HUGLA, Robert NGO, Catherine ARABEYRE-FABRE, Viviane MEUNIER, Freddy SADOUN, Olivier FEDELI, Martine RIVAL, Martine BOURRIE, François GUILLOU, Patrick MAUREL and Gérard FABRE

SANOFI-AVENTIS RECHERCHE (SK, SH, RN, CA-F, VM, FS, OF, MB, FG, GF)

Department of Discovery Metabolism, Pharmacokinetics and Safety (DMPK-S)

371 Rue du Professeur Joseph Blayac

34184 Montpellier, Cedex 4, France

SANOFI-AVENTIS RECHERCHE (MR)

Department of Chemical and Analytical Sciences,

195, Route d'Espagne

31036 Toulouse, Cedex, France

INSERM U632 (PM)

1919, Route de Mende

34293 Montpellier, Cedex 05, France

DMD #19539

Running title: *In vitro* direct *N*-glucuronidation of Midazolam

Corresponding author:

Gérard FABRE

Department of Discovery Metabolism, Pharmacokinetics and Safety (DMPK-S)

Sanofi-Aventis

371 Rue du Professeur Joseph Blayac

34184 Montpellier, Cedex 4

France

Tel: 33 (0)4 99 77 64 64

Fax: 33 (0)4 99 77 54 91

E-Mail: gerard.fabre@sanofi-aventis.com

Number of text pages: 43

Number of tables: 7

Number of figures: 16

Number of references: 41

Number of words in the Abstract: 248

Number of words in the Introduction: 929

Number of words in the Discussion: 736

Abbreviations:

CYP, cytochrome P450; DDI, drug-drug interactions; DMSO, dimethyl sulfoxide; ESI, electrospray ionization mode; HPLC-UV, high-performance liquid chromatography coupled with ultra-violet detection; Glu-O-MDZ, 1'-hydroxymidazolam glucuronide; 1'-OH-MDZ, 1'-hydroxymidazolam; 4-OH-MDZ, 4-hydroxymidazolam; LC-MS/MS, liquid chromatography/tandem mass spectrometry; MDZ, midazolam; *N*-Glu, *N*-glucuronide; NMR, nuclear magnetic resonance; SPE, solid phase extraction; HPLC-UV-SPE-NMR, high-performance liquid chromatography with coupled ultra-violet detection, solid phase extraction and nuclear magnetic resonance; TFA, Trifluoro acetic acid; UDPGA, Uridine 5'-diphosphoglucuronic acid; UGT, UDP-glucuronosyl transferase

Abstract

Midazolam is one of the most commonly used *in vivo* and *in vitro* CYP3A4 probe substrate for drug-drug interactions (DDI) studies. The major metabolic pathway of midazolam in humans consists in the CYP3A4 mediated 1'-hydroxylation followed by urinary excretion as 1'-*O*-glucuronide derivative. In the present study, following incubation of midazolam with human liver microsomes supplemented with UDPGA, two major HPLC peaks were isolated. HPLC and LC-MS/MS analyses identified these two metabolites as quaternary direct *N*-glucuronides of midazolam thus revealing an additional metabolic pathway for midazolam. ^{1}H NMR spectrometry studies were performed demonstrating that these two glucuronides were β-*N*-glucuronides, which could be considered as two different conformers of the same molecule. According to molecular modelling experiments, the two glucuronide derivatives could be involved in atropoisomerism equilibrium. The formation of midazolam *N*-glucuronide exhibited moderate intersubject variability (at most 4.5-fold difference, n = 10). Among the recombinant human UGTs isoforms tested, only isoform UGT1A4 catalyzed the *N*-glucuronidation of midazolam fitting a Michaelis-Menten model. K_m and V_{max} values were of 29.9 ± 2.4 µM and 659.6 ± 19.0 pmol/min/mg protein, respectively. The *N*-glucuronide derivative was found in human hepatocytes incubated under control conditions but also in the presence of the well-known CYP3A4 inhibitor, ketoconazole. In the context of the *in vitro* study of CYP3A4-mediated DDI using midazolam and ketoconazole, direct midazolam *N*-glucuronidation may partly compensate the decrease in midazolam metabolic clearance caused by the addition of the inhibitor thus potentially leading to under-estimation, at least *in vitro*, of the extent of DDI.

Introduction

Because large number of currently available drugs and future drugs will be metabolized by the members of the CYP3A subfamily the potential for drug-drug interaction (DDI) is substantial. Drug-drug interactions involving the inhibition and induction of CYP3A4 are of great scientific and clinical relevance. Indeed, drugs with potent CYP3A4 inhibitory properties have been implicated in significant CYP3A4-mediated DDIs. Interaction of the benzodiazepines with the azole antifungal agents and especially the inhibition of CYP3A-mediated midazolam metabolism by ketoconazole have been widely studied. Concomitant administration of both drugs results in large, variable and highly significant increases (5- to 16-fold) in midazolam exposure, depending on the dose regimen of ketoconazole used. Table 1 summarizes available clinical data on the effects of ketoconazole on midazolam plasma levels following oral or intravenous administration of midazolam.

Midazolam is a short-acting water-soluble imidazo-benzodiazepine (Figure 1) extensively used in clinical practice mainly for induction and maintenance of anesthesia, sedation for diagnostic and therapeutic procedures and also as an oral hypnotic agent (Reves, et al., 1985). Midazolam is a well-known CYP3A substrate since its metabolism has been the focus of many *in vitro* investigations (Fabre, et al., 1988a; Kronbach, et al., 1989; Wrighton and Ring, 1994; Ghosal, et al., 1996; Maenpaa, et al., 1998; Hosea, et al., 2000; Wang, et al., 2000). Midazolam biotransformation is mediated by at least three different CYP3A isoenzymes: 3A4, 3A5 and 3A7 (Gorski, et al., 1994; Kuehl, et al., 2001). Since CYP3A7 is principally expressed in fetal tissues, CYP3A4 and CYP3A5 represent the main CYP isoforms in adult liver and intestine (Guengerich, 1995).

Midazolam biotransformation yields two primary hydroxylated metabolites: 1'-hydroxy-midazolam and 4-hydroxy-midazolam. 1'-hydroxy-midazolam represents the main metabolite since it accounts for 95 % of net intrinsic clearance of midazolam in human liver

microsomes (von Moltke, et al., 1996). *In vivo*, when administered orally to man, midazolam is rapidly absorbed and the amount of 1'-hydroxy-midazolam excreted as conjugate in the urine of healthy volunteers reaches 75 % of the initial administered dose *versus* 4 % for the minor primary metabolite, 4-hydroxy-midazolam and 6 % for a minor secondary metabolite 1',4-dihydroxy-midazolam. Both metabolic routes are also catalyzed by CYP3A4 and hydroxylated metabolites are excreted as glucurono-conjugates (Heizmann and Ziegler, 1981; Dundee, et al., 1984).

In recent years, midazolam has emerged as one of the best and most widely used *in vitro* and *in vivo* metabolic probe for prediction of CYP3A activity (Thummel and Wilkinson, 1998; von Moltke, et al., 1996; Galetin, et al., 2005) because it meets most, if not all, of the necessary criteria suggested for such applications. Indeed, midazolam is a substrate of one single and well-known P450 isoform, it is highly sensitive to changes in status/activity of the respective P450 enzyme, it is unaffected by P-glycoprotein or other known transporters and presents negligible pharmacodynamic effects (adverse effects) at the dose used for probe studies (Bjornsson, et al., 2003). In addition, midazolam is commercially available, exhibits suitable pharmacokinetic profile and can be administered both orally and intravenously. Midazolam can provide a measure of CYP3A4/5 activity relative to both intestinal and hepatic metabolism. Tables 2 and 3 list the preferred *in vitro* and *in vivo* CYP3A4 probe substrates, inhibitors and inducers recommended by the U.S. Food and Drug Administration (FDA) Guidance for Industry ("Drug Interaction Studies – Study Design, Data Analysis and Implications for Dosing and Labelling") released in September 2006.

In vitro inhibition of human liver microsomal metabolism of midazolam to 1'-hydroxy-midazolam by ketoconazole was initially studied by Gascon and Dayer (1991). Wrighton and Ring (1994) described ketoconazole as a potent, selective and non-competitive inhibitor with K_i ranging between 0.0037 and 0.18 μM according to the authors (Bourrié, et

al., 1996; von Moltke, et al., 1996; Galetin, et al., 2005). Therefore, plasma C_{max} concentrations of ketoconazole which can be as high as 25 µM in humans, is expected to be a potent inhibitor of metabolism of all CYP3A substrates thus causing very significant CYP3A4-mediated drug-drug interactions *in vivo*.

Midazolam and ketoconazole are therefore extensively used both *in vitro* and *in vivo* for the prediction of CYP3A-mediated DDIs, the former as a phenotypic marker of CYP3A4/5 metabolic capacity, the latter as a reference as specific and potent CYP3A4/5 inhibitor. The central hypothesis for the prediction of DDIs involving CYP3A4 inhibition by a compound of interest, both *in vitro* and *in vivo*, is that the decrease in the overall observed clearance of midazolam caused by the co-administration of (or *in vitro* co-incubation with) a CYP3A4 inhibitor, *i.e.* ketoconazole or other novel compounds exhibiting CYP3A4 inhibitory potency. This can be assigned entirely and exclusively to the CYP3A4/5 enzymes and therefore can be used to predict the magnitude of the clinical interaction expected between the potential inhibitor under investigation and any other co-administered CYP3A4 substrate.

However, *in vitro* studies showed that midazolam could also be directly conjugated with UDPGA (Siddle, et al., 2003). Moreover, additional experiments conducted in our laboratory demonstrated that ketoconazole did not fully inhibit the *in vitro* metabolic clearance of midazolam in human hepatocytes. Such results would suggest that, at least *in vitro*, the metabolism of midazolam is not exclusively dependent on CYP3A4/5 thus warranting further investigation of midazolam metabolic pathways and of the ketoconazole / midazolam metabolic interaction.

The purpose of the present work was to study in more details the *in vitro* metabolic pathways of midazolam in humans and to elucidate whether or not an alternative metabolic route such as direct *N*-glucuronidation could be responsible for a metabolic shift between CYP3A4/5 and

UGT, thus possibly leading to a certain extent of misinterpretation of DDI study results both *in vitro* and *in vivo*.

Materials and Methods

Compounds

Midazolam (MDZ; 8-Chloro-6-(2-fluorophenyl)-1-methyl-4H-imidazo [1,5a] [1,4] benzodiazepine) and its hydroxylated 1'-hydroxymidazolam (1'OH-MDZ; 8-Chloro-6-(2-fluorophenyl)-1-hydroxymethyl-4H-imidazo [1,5a] [1,4] benzodiazepine) metabolite were purchased from Ultrafine Chemicals (Oxford, UK). The 1'-hydroxymidazolam glucuronide (Glu-O-MDZ) was synthesized by the Isotope Chemistry and Metabolites Synthesis Department of Sanofi Aventis Recherche (Chilly-Mazarin, France). Dimethyl sulfoxide (DMSO), Ketoconazole, Uridine 5'-diphosphoglucuronic acid (UDPGA), alamethicin, ethanolamine, transferrin, linoleic acid, ascorbic acid, insulin, L-arginin and glucagon were obtained from Sigma (St Louis, MO). Ham F12 and Williams E media, L-glutamine, HEPES, sodium pyruvate, penicillin, and streptomycin were purchased from Invitrogen (Carlsbad, CA). The other chemicals and solvents used were all of analytical grade.

Reagents

Recombinant human UGTs (Supersomes^{TM}: UGT1A1, UGT1A3, UGT1A4, UGT1A6, UGT1A7, UGT1A8, UGT1A9, UGT1A10, UGT2B4, UGT2B7, UGT2B15 and UGT2B17) expressed in baculovirus-infected insect cells and control microsomes from insect cells infected with wild-type baculovirus were all obtained from BD Gentest (Woburn, MA, USA).

Identification of Midazolam N-glucuronides by High Performance Liquid Chromatography-Electrospray Ionization Mass Spectrometry (HPLC-ESI- MS ^{n})

Chromatography was performed with an HPLC system Agilent 1100 (Agilent, Santa Clara, CA, USA) which was equipped with a reverse phase column (SunFire C_{18} 3.5 µm particle size, 3.0 i.d. x 150 mm length, Waters Milford, MA). The column temperature was set at 35°C

using a column oven. The mobile phase was composed of (A) distilled water with 0.1 % (v/v) formic acid and (B) acetonitrile/methanol (70/30), (v/v). Elution was performed using the following gradient of solvent B: 0 - 5 min at 15 % then 55 % over 20 minutes. The flow rate was 0.4 mL/min. Under these analytical conditions, the retention time for MDZ was 14.8 minutes. The column outlet was connected to a Finnigan Linear ion Trap mass spectrometer (Thermo Finnigan MAT, San Jose, CA) operating in electrospray positive ionization mode.

Preparation of M1 and M2

After a 3-hour incubation period of 98 µg Midazolam with recombinant UGT1A4 in the presence of UDPGA, the HPLC eluate containing all the Midazolam-*N*-glucuronides converted from Midazolam was collected. At the end of this process, the total amount estimated for metabolites M1 and M2 was approximately 50 µg. These metabolites were in solution in a water/acetonitrile (50/50, v/v) mixture.

On-Line Nuclear Magnetic Resonance

The HPLC-UV-SPE-NMR measurements were carried out using an Agilent 1100 series chromatographic system (auto-sampler, degasser, quaternary pump, oven and UV Variable Wavelength Detector), a Prospekt 2 Solid Phase Extraction robot (Bruker Biospin, Rheinstetten, Germany and Spark Holland, Emmen, Holland) and an AVANCE 500 NMR spectrometer (Bruker Biospin, Wissembourg, France). Injections were performed by auto-sampler into a reverse phase HPLC column. M1 and M2 were automatically detected by UV absorbance and trapped onto SPE cartridges after post-column addition of water. Then, the metabolites present in M1 and M2 peaks were flushed to the NMR flow-cell to record NMR spectra.

HPLC-UV conditions; the chromatography was controlled using the HyStar 2.3 software (Bruker Daltonik, Rheinstetten, Germany). Elution was performed using eluent A (water, Carlo Erba + 0.01 % TFA) and eluent B (Acetonitrile, Riedel de Haen, Germany. The initial

conditions consisted of 20 % eluent B and 80 % eluent A. The flow rate was set at 0.4 mL/min through an Inertsil ODS-3 C_{18} 2.1 mm i.d., 150 mm length, 5 µm particle size HPLC column (GL Sciences, USA). The column temperature was maintained in an oven at 20°C. Gradient elution was performed using eluents A and B with the following gradient: 20 % B to 25 % B in 20 minutes, 25 % B to 90 % B in 2 minutes, 90 % B held for 3 minutes and post time of 2 minutes under initial conditions. The M1/M2 solution was dried under N_2 stream. The total amount of M1/M2 mixture recovered was estimated to be approximately 25 µg (estimated recovery of 50 %). The dried extract was then dissolved in DMSO (100 µL). 10 µL of this M1/M2 solution were injected. UV wavelength detection was set at 254 nm. Retention times observed for metabolites M1 and M2 were 6.62 min and 6.92 min, respectively.

SPE conditions; the Prospekt 2 solid phase extraction robot was controlled using the BRUKER HyStar 2.3 software. The type of SPE cartridge used was Hysphere GP (2 mm i.d., 10 mm length, 10-12 µm particle size). Prior to use, the cartridge was cleaned with acetonitrile and conditioned with water. The post-column water make-up flow was set at 0.8 mL/min, and was performed using a K100 HPLC pump (Knauer, Berlin, Germany). The total flow going through the trapping cartridge was 1.2 mL/min. A 4-step trapping process (4*10 µL injected) was carried out for each metabolite M1 and M2 in order to increase the amount of compound available for NMR experiments. The peak of interest was automatically detected by UV absorbance at 254 nm for trapping. Trapped M1 and M2 were dried under a stream of N_2 for 40 min to remove residual solvents. Pure deuterated acetonitrile ("100% grade", Eurisotop, France) was used to flush M1 and M2 from the SPE cartridges directly into the NMR cell for spectroscopic analysis.

NMR conditions; from the SPE cartridges, trapped compounds were eluted into a BRUKER AVANCE 500 MHz spectrometer operating at 500.13 MHz for proton and equipped with a 3 mm $^{1}H/^{13}C$ probe, inverse and gradient z, fitted with a 60 µL flow cell (30 µL active volume).

The NMR was controlled using XwinNMR and IconNMR softwares (Bruker Daltonik, Rheinstetten, Germany). The concentrated metabolites M1 and M2 flushed in the flow probe were of sufficient purity and quantity to provide ^{1}H 1D data, as well as ^{1}H 2D homonuclear polarization transfer spectrum.

The ^{1}H 1D proton spectrum was recorded in 1024 scans, using a 64 K transient and a spectral width of 10330 Hz (acquisition time 3.17 s). The data were apodized with an exponential window function (0.3 Hz). The COSYGPQF spectrum was obtained with F_2 and F_1 spectral widths of 6666 Hz in 2 K data points for 177 t_1 increments and 128 scans per t_1. The data were apodized with a sine bell window function in both dimensions and zero-filled in the F_1 dimension to 512 data points. The ^{1}H NMR spectra were calibrated on acetonitrile signal (1.95 ppm)

Off-Line NMR

HPLC-UV-MS experiments were performed to collect M1 and M2 metabolites. These compounds were collected using an Agilent 1100 series chromatographic system (auto sampler, binary pump, oven, UV Variable Wavelength Detector, and fraction collector), a Mass Spectrometer (quadrupole Agilent 6110, CA, USA), and an AVANCE 600 NMR spectrometer (Bruker Biospin, Wissembourg, France). Metabolites M1 and M2 were automatically detected by MS, collected into vials and dried under N_2. Then, metabolites M1 and M2 were put in solution, and NMR spectra were recorded.

HPLC conditions; the chromatography was controlled using the Agilent LC/MSD Chemstation software. Elution was peformed using eluent A (water, Carlo Erba) and eluent B (acetonitrile/methanol, 70/30). The initial conditions consisted of 10 % eluent B and 90 % eluent A. The flow rate was set at 0.4 mL/min through an YMC-Pack J'Sphere H80 2.1 mm i.d., 250 mm length, 4 µm particle size HPLC column (GL Sciences, USA). The column temperature was maintained in an oven at 30°C. Gradient elution was performed using eluent

A and B with the following gradient: 10 % B to 28 % B in 2 minutes, 28 % B held for 16 minutes, 28 % B to 50 % B in 1 minute and post time of 5 minutes under initial conditions. M1/M2 solution underwent an evaporation process to remove the major part of acetonitrile. The total amount of M1/M2 was estimated to be 50 µg in solution in water. 50 µL (containing approximately 2.5 µg of M1/M2) of this solution were injected for the chromatographic run.

M1 and M2 collection conditions; HPLC, MS and fraction collector were controlled using the Agilent LC/MSD Chemstation software. After the HPLC column the flow was split in a ratio of 10/90 (10% MS and 90 % fraction collector). Metabolites M1 and M2 were detected using the MS trace in SIM mode (*m/z* 502) recorded by an Agilent quadrupole 6110 mass spectrometer (Agilent, Santa Clara, CA, USA) equipped with ESI source. Retention times observed for metabolites M1 and M2 were 11.2 min and 11.8 min, respectively. Elution peaks of metabolites M1 and M2 were collected using an Agilent 1200 fraction collector. This purification process was repeated 20 times. At the end of this process, M1 and M2 were isolated and kept in solution (28 % B and 72 % A). The M1 and M2 solutions were dried under N_2 stream. The amount of each metabolite M1 and M2 was estimated to be 10 µg.

NMR conditions; the dried extracts containing the metabolites M1 and M2 were reconstituted in DMSO-D_6 (Deuterated Dimethyl Sulfoxide, "100% grade", Eurisotop, France). Approximately 10 µg of each metabolite M1 and M2 were dissolved in 30 µL of DMSO-D_6. 1,7 mm capillary NMR tubes were filled up with these solutions to perform NMR experiments. 10 mg of Midazolam was also dissolved in 600 µL of DMSO-D_6 and put into 5 mm NMR tube in order to compare M1/M2 metabolites and Midazolam NMR data. Spectra were recorded using a BRUKER AVANCE 600 MHz spectrometer operating at 600.13 MHz for proton (150.91 MHz for ^{13}C) and equipped with a 5 mm TCI $^{1}H/^{13}C$, inverse and gradient z, Cryoprobe^{TM}. The concentrated metabolites in the cryoprobe were of sufficient purity and

DMD Fast Forward. Published on February 6, 2008 as DOI: 10.1124/dmd.107.019539
This article has not been copyedited and formatted. The final version may differ from this version.

quantity to provide ^{1}H data, as well as 2D homonuclear and heteronuclear polarization transfer spectra.

For Midazolam, the ^{1}H 1D proton spectrum was recorded in 64 scans, using a 48 K transient and a spectral width of 7861 Hz (acquisition time 3.12 s). The data were apodized with a Gaussian window function (-0.3 Hz, 0.1) and zero-filled (64 K). The ^{1}H 2D COSYGPQF spectrum was obtained with an F_2 and F_1 spectral width of 1796 Hz in 6 K data points for 256 t_1 increments and 4 scans per t_1. The data were apodized with a sine bell window function in both dimensions and zero-filled in the F_1 dimension to 2048 data points. The $^{1}H/^{13}C$ 2D HSQCEDETGPSI spectrum was obtained with F_2 spectral width of 4807 Hz in 3 K data points for 256 t_1 increments and 4 scans per t_1. The data were apodized with a shifted ($\pi/2$) sine bell window function in both dimensions. NMR spectra were calibrated on DMSO-D_6 signal (2.5 ppm for ^{1}H and 39.6 ppm for ^{13}C).

For M1 and M2 metabolites, the ^{1}H 1D proton spectra were recorded in 2048 scans, using a 48 K transient and a spectral width of 7861 Hz (acquisition time 3.12 s). The data were apodized with an exponential window function (0.3 Hz) and zero-filled (64 K). The ^{1}H 2D COSYQF spectrum was obtained with an F_2 and F_1 spectral width of 5388 Hz in 4K data points for 512 t_1 increments and 64 scans per t_1. The data were apodized with a sine bell window function in both dimensions and zero-filled in the F_1 dimension to 2048 data points. The $^{1}H/^{13}C$ 2D HSQCEDETGPSI spectrum was obtained with an F2 spectral width of 4807 Hz in 2 K data points for 256 t_1 increments and 112 scans per t_1. The data were apodized with a shifted ($\pi/2$) sine bell window function in both dimensions. NMR spectra were calibrated on DMSO-D_6 signal (2.5 ppm for ^{1}H and 39.6 ppm for ^{13}C).

Molecular modelling

All molecular modelling work was done with the MMF94 force field, which is part of SYBYL environment (TRIPOS, USA).

Human liver microsomes and human hepatocytes

Liver samples were obtained either from whole livers coming from human donors that were unfit for organ transplant or from donors undergoing partial hepatectomy. These liver samples were termed "HTL-x, FH-x or HL-x". Available demographic information for patients including gender and age are reported in Tables 4 and 5.

Liver microsomes preparation

Microsomes were prepared from ten donors using standard techniques adapted by Fabre *et al.*, (1988b). Briefly, microsomes were prepared from frozen liver samples by differential ultra-centrifugations. Microsomal pellets were resuspended in 0.1 M potassium phosphate buffer containing 0.1 mM EDTA and 20 % glycerol (v/v), aliquoted and stored at -80°C until use. Protein content was determined by the method of Bradford as described by Pollard (1978). Cytochrome P450 content was estimated from the CO difference spectrum as described by Omura and Sato (1964). Frozen microsomes were thawed only once just prior to use.

Cell isolation procedure for human hepatocytes primary culture

Tissue samples were rapidly transported from the operating theatre in ice-cold University of Wisconsin solution at 4° C. Hepatocytes were obtained according to the two-step collagenase perfusion technique described by Fabre *et al.* (1988a). This perfusion technique allows several billions of cells to be obtained, up to 4 x 10^9 hepatocytes depending on the size of the liver sample. Following different washing steps (filtration through 150 and 250 µm nylon mesh, and low speed centrifugation at 50 x g for 5 minutes, three-fold), freshly isolated hepatocytes were plated on collagen-coated plastic dishes in a chemically-defined medium adapted from Isom and Georgoff (1984), consisting in a 50/50 (v/v) mixture of Ham F12/Williams E medium supplemented with 10 % decomplemented fetal calf serum, 10 mg/L insulin, 0.8 mg/L glucagon and antibiotics (100 IU penicillin and 100 µg/mL streptomycin). Viability for all human hepatocyte preparations used was greater than 85 % as measured by Trypan blue

DMD Fast Forward. Published on February 6, 2008 as DOI: 10.1124/dmd.107.019539
This article has not been copyedited and formatted. The final version may differ from this version.

exclusion test. Hepatocytes were seeded in 6-well plates with 1.4 x 10^6 hepatocytes in a final volume of 1 mL. After 4 to 6 hours of incubation at 37°C in a 5 % CO_2 and 100 % humidified atmosphere, period during which hepatocytes attached to the collagen-matrix, plating medium was removed and replaced by the same serum-free culture medium supplemented with HEPES (3.6 g/L), ethanolamine (4 mg/L), transferrin (10 mg/L), linoleic acid-albumin (1.4 mg/L), glucose (252 mg/L), sodium pyruvate (44 mg/L), ascorbic acid (50 mg/L), arginine (104 mg/L) and L-glutamine (0.7 g/L).

Midazolam N-glucuronidation assay in human liver microsomes

The assay mixture was composed of human liver microsomes (1 $mg.mL^{-1}$), UDPGA (3 mM), 100 mM potassium phosphate (pH 7.4) containing 5 mM $MgCl_2$, alamethicin (25 $\mu g.mL^{-1}$) and 100 µM MDZ dissolved in DMSO in a final volume of 500 µL. The final concentration of DMSO in the reaction mixture was 0.1 % (v/v). Initial rate conditions with respect to time and protein concentration for the formation of the MDZ-*N*-glucuronides were established in preliminary studies. The reaction was initiated by addition of 50 µL of an aqueous solution of 30 mM UDPGA, incubated at 37°C and stopped after 60 minutes by addition of one volume ice-cold acetonitrile. After removal of the protein by centrifugation at 10,000 rpm for 5 minutes, a portion of the supernatant was analyzed by HPLC.

Midazolam N-glucuronidation by human recombinant UGT enzymes

The assay mixture was composed of the microsomes (1 $mg.mL^{-1}$) of baculovirus-infected cells expressing human UGTs, 100 mM potassium phosphate (pH 7.4) containing 5 mM $MgCl_2$, alamethicin (25 $\mu g.mL^{-1}$), UDPGA (3 mM) and 100 µM MDZ in a final volume of 500 µL. The reaction was initiated by addition of 50 µL of an aqueous solution of UDPGA, incubated at 37°C and stopped after 60 minutes by addition of one volume ice-cold acetonitrile. After removal of the protein by centrifugation at 10,000 rpm for 5 minutes, a portion of the supernatant was analyzed by HPLC.

DMD Fast Forward. Published on February 6, 2008 as DOI: 10.1124/dmd.107.019539
This article has not been copyedited and formatted. The final version may differ from this version.

Metabolic studies using fresh human hepatocytes in primary culture

Experiments were performed in 6-well plastic plates coated with rat tail Collagen type I. Once medium was renewed, 5 µM of MDZ was directly added to the incubation medium in the absence or the presence of 10 µM ketoconazole. Regardless of the final concentration investigated, the final solvent (DMSO) concentration never exceeded 0.2 % (v/v). To determine the metabolism of MDZ, kinetic studies were performed over 6 to 8 hours, based on primary determinations on the rate of MDZ biotransformation. For each time point, one mL of acetonitrile was added to the specific well for protein precipitation, and both extracellular medium and cell compartment were scraped together. Cell extracts were transferred to a glass tube and stored at -20°C until analysis. Before analysis, cell homogenates were sonicated for a few seconds, homogenized and centrifuged at 6,000 x *g* for 30 minutes. Supernatant fluids were then analyzed for unchanged MDZ and its specific metabolites.

HPLC Instruments and Analytical conditions

HPLC analysis was performed using a Waters 2795 Alliance HPLC system (Waters, Milford, MA) equipped with a Waters UV detector 2487 and a Waters Symmetry C_{18} column (250 length x 4.6 mm i.d.; 5 µm particle size). The column temperature was 35°C and the eluate was monitored by ultraviolet absorbance at 250 nm. Solvent A was 0.1 % (v/v) formic acid with 2 % ammonium acetate (w/v) in distilled water. Solvent B was a mixture of aetonitrile/methanol (70/30, v/v), 0.2 % formic acid (v/v), 1 % water (v/v) and 0.15 % ammonium acetate (w/v). A linear gradient of 15 to 55 % mobile phase B over 23 minutes was used for analysis of MDZ and its metabolites at a flow rate of 0.9 mL/min. The retention times of MDZ, 1'-OH-MDZ, MDZ-*O*-Glu and midazolam-*N*-glucuronide conjugates (*N*-Glu) were 20.6, 22.6, 18, 16.9 and 17.8 minutes, respectively. Due to the absence of authentic standards for midazolam-*N*-glucuronides, these conjugates were semi-quantified using a

midazolam calibration curve, after verification that their UV absorbance was equivalent to that of MDZ. To do so, the HPLC peaks containing midazolam-*N*-glucuronides obtained from the quantitative conversion of midazolam by recombinant UGT1A4 incubates were collected. After hydrolysis of midazolam-*N*-glucuronides to midazolam, the peak area ratio of MDZ to the converted midazolam-*N*-glucuronides was found to be 1, thus allowing the quantification of MDZ-*N*-glucuronides using MDZ standard curves.

Data analysis

The kinetic parameters K_m and V_{max} were calculated using GraFit v5 software.

The intrinsic *in vitro* metabolic clearances (Cl_{int}) were calculated using WinNonLin PK analysis software. All disappearance kinetics data were fitted with a model using the following equation:

$$\mathbf{Cl_{int} = Dose/AUC_{(0\text{-}Clast)}}$$

Results

Identification of Midazolam N-glucuronides formed by Human Liver Microsomes by HPLC-ESI-MS^n Analysis

Enzymatic formation of midazolam *N*-glucuronides by human liver microsomes was first characterized by HPLC-UV and HPLC-ESI-MS^n. Figure 2 shows representative HPLC-UV chromatograms of midazolam and enzymatically formed midazolam-*N*-glucuronides (M1 and M2) by human liver microsomes in the presence of UDPGA. Figures 3*a*, 3*b* and 3*c* show the mass spectra of midazolam and both *N*-glucuronides with a pseudomolecular ion $[MH]^+$ at m/z = 326 and molecular ions $[M]^+$ at m/z = 502 (addition of 176 Da), respectively. The MS^2 mass spectra of both glucuronides (Figures 3*d* and 3*e*) show only one fragment ion at 326 m/z (loss of 176 Da) corresponding to the aglycone ion. The MS^3 mass spectra of both glucuronides (Figures 3*f* and 3*g*) are similar and showed the same major fragment ions at *m/z* = 244, 291 and 325, characteristic of MS^2 mass spectra of midazolam (Figure 3*h*).

From these observations, it was confirmed that the peaks labeled “M1” and “M2” formed by incubation of midazolam with human liver microsomes in the presence of UDP-glucuronic acid were consistent with midazolam direct glucuronide derivatives. Furthermore, in the absence of free hydroxyl group in the structure of midazolam, these MDZ-glucuronides were most likely MDZ-*N*-glucuronide derivatives.

Nuclear Magnetic Resonance studies

Approximately one hour after purification of M1 and M2 (OFF LINE NMR), these metabolites were analyzed using LC-MS/MS in order to check the purity of each sample. Interestingly, the sample corresponding to metabolite M1 (> 90 % purity upon collection) already contained a mixture of both M1 and M2 in equal proportions (50/50). Similarly, the sample corresponding to metabolite M2 (also > 90 % purity upon collection) was also composed of a M1/M2 mixture, also in equal proportions (50/50). These results seemed to

DMD Fast Forward. Published on February 6, 2008 as DOI: 10.1124/dmd.107.019539
This article has not been copyedited and formatted. The final version may differ from this version.

indicate that the two metabolites M1 and M2 were in equilibrium, and could not be kept separated in solution for a long period of time. On the other hand, ^{1}H 1D NMR spectra recorded for each purified metabolite M1 and M2 (OFF-LINE NMR) were very similar, and corresponded to the superimposition of M1 and M2 NMR spectra in equal proportions (50/50). Moreover, the observation of ^{1}H 1D NMR spectrum of the M1/M2 mixture (ON-LINE NMR and OFF-LINE NMR) showed that these two compounds shared the same basic structure. This result confirmed that metabolites M1 and M2 were in equilibrium, and as their structure was likely to be the same, it was postulated that M1 and M2 were two conformers of the same *N*-glucuronide derivative of midazolam.

The ^{1}H 1D NMR spectra of M1/M2 metabolites (Figure 4, ON-LINE NMR) showed significant signals of glucuronide moiety (Ismail, et al., 2002) at δ = 5.46 ppm and δ = 5.50 ppm (anomeric protons 17 of the two conformers), at δ = 3.61 (18), at δ = 3.52 /3.54 (19), δ = 3.61 (20) and δ = 4.1 (21). The β-anomeric configuration was assigned to M1 and M2 glucuronide conjugates because the coupling constants of their anomeric protons were approximately 8.5 Hz. Coupling constants in the range of 7 to 10 Hz have been reported to be characteristic of the β-anomers of various glucuronides, whereas the α-anomers have coupling constants in the range of 2 to 4 Hz (Kemp, et al., 2002).

The comparison of ^{1}H 1D NMR spectra of M1/M2 and midazolam (Table 4, OFF-LINE NMR) showed that resonances corresponding to each proton of midazolam were also present in the structures of M1 and M2. This information suggested that the glucuronide group was linked to one of the N atoms (2, 5 and 11) present in the chemical structures of M1 and M2.

Assignments of the resonances of midazolam, and M1/M2 metabolites are showed in Table 6.

The positioning of the glucuronide ring on N atom (5) was not in agreement with the chemical shifts observed for proton (4) in metabolites M1 and M2. Indeed, a positive charge located on this N atom (5) should have induced a movement of proton (4) chemical shifts towards lower

DMD Fast Forward. Published on February 6, 2008 as DOI: 10.1124/dmd.107.019539
This article has not been copyedited and formatted. The final version may differ from this version.

field. This phenomenon was not observed, as seen in Table 6 where proton (4) chemical shifts of metabolites M1 and M2 and midazolam are all similar.

The major differences observed between midazolam and metabolites M1/M2 NMR chemical shifts were focused on the imidazole proton (3) and methyl group (12). We noticed that proton (3) and methyl group (12) chemical shifts were located at lower field for metabolites M1/M2. Furthermore, proton (3) and methyl group (12) both showed duplicate signals, one for each supposed conformer M1 and M2 (Figure 5). Finally, we assumed that the hybridization type for atoms N (11) and N (2) located in the imidazole ring was sp^2 as it is usually supposed. Thus, a conjugation of the glucuronide ring with the N atom (11) would be unlikely. These observations taken into account, we assumed that the glucuronide ring was located on N atom (2) for metabolites M1 and M2. Moreover, due to the inter-conversion described above between M1 and M2, it was also proposed that these two metabolites M1 and M2 should be considered as two conformers in equilibrium.

Variable temperature NMR experiments were performed to probe the torsional barrier. Unfortunately, metabolites M1/M2 underwent thermal decomposition during this study and under these conditions we could not observe NMR signal collapses for protons (3), (17) and (12), as it was expected. Subsequently, Nuclear Overhauser experiments (^{1}H 2D NOESY) were also performed, in order to help discriminate the two conformers M1 and M2. Unfortunately, poor sensitivity due to the low amount of metabolites did not allow observing any signals.

In order to understand better the likely equilibrium which affected NMR and LC-MS/MS spectra during this study, *i.e.*, the presence of some duplicate NMR signals and the impossibility to keep M1 and M2 separate after LC purification, molecular modelling calculations were carried out. During this work, we assumed that the hybridization types for atoms N (2) and N (11) in the imidazole ring were sp^2. NMR data recorded during this study

suggested that metabolites M1 and M2 should be considered as conformers in equilibrium (50/50). The glucuronide ring is linked to the imidazole ring with covalent Nitrogen–Carbon bond, a type of chemical bond which is known to undergo atropoisomerism. Atropoisomerism (Schantl, 1995; Voitenko, et al., 2002; Campos, et al., 1999) is a type of stereoisomerism that may arise in systems where free rotation around a single covalent bond is sufficiently impeded to allow different stereoisomers to be isolated. For metabolites M1 and M2, we assumed that the glucuronide ring located on atom N (2) of the imidazole ring underwent a restricted rotational motion around the Nitrogen–Carbon bond. Molecular modelling experiments confirmed the presence of a torsional barrier around the Nitrogen-Carbon bond which connects the imidazole ring to the glucuronide ring. Profiles for changes in energy rotation displayed maxima when the glucuronide ring was passing through the region of the methyl group (12) located on the imidazole ring. Minima energy profiles were found for two energy conformers, when the glucuronide ring approximately bisected the imidazole ring plane, being perpendicular to this plane. Furthermore, the calculated relative populations of these two low energy conformers were in reasonably good agreement with the corresponding abundances observed for each conformer M1 and M2 (atom 3, about 50/50, Figure 5). Finally, the energy of the torsional barrier was estimated to 20 $Kcal.mol^{-1}$, in agreement with atropoisomerism phenomena previously described in the literature (Srivastav, et al., 1993).

In conclusion, the whole set of NMR data and molecular modelling calculation, were in accordance with the proposed structure shown below for metabolites M1 and M2 (Figure 6).

Altogether, these results allowed us to propose a new metabolic scheme for midazolam as shown in Figure 7.

Midazolam N-glucuronidation in human liver microsomes

Formation rates of Midazolam *N*-glucuronide conjugates were determined in liver microsomes of ten different human donors, at an initial substrate concentration of 100 µM. A

DMD Fast Forward. Published on February 6, 2008 as DOI: 10.1124/dmd.107.019539
This article has not been copyedited and formatted. The final version may differ from this version.

moderate variability between individual donors was observed as shown in Figure 8. All liver samples were able to glucurono-conjugate midazolam but preparation HTL19 exhibited the highest glucuronidation capacity, 4.5-fold faster than HL23, the slowest one. Since additional physico-chemical and ^{1}H NMR experiments demonstrated a very rapid equilibrium between both conformers, *N*-glucuronide quantification was performed by summing the two conformers M1 and M2 together.

Midazolam N-glucuronidation by recombinant human UGT enzymes

All human recombinant UGT isoforms expressed in baculovirus-infected insect cells (UGT1A1, UGT1A3, UGT1A4, UGT1A6, UGT1A7, UGT1A8, UGT1A9, UGT1A10, UGT2B4, UGT2B7, UGT2B15 and UGT2B17) which were commercially available were compared with regard to their ability to catalyze Midazolam *N*-glucuronidation. Among them, only recombinant UGT1A4 showed significant Midazolam *N*-glucuronosyltransferase activity (Figure 9).

Kinetic parameters for Midazolam N-glucuronidation by human liver microsomes and recombinant UGT1A4

Kinetic analyses of Midazolam *N*-glucuronidation were performed using human liver microsomes (from donor HTL19) and recombinant UGT1A4. Midazolam *N*-glucuronidation displayed Michaelis-Menten kinetics. Figure 10 shows the concentration-dependent formation rate of Midazolam *N*-glucuronide in human liver microsomes and recombinant UGT1A4, respectively. Observed apparent K_m and V_{max} values for microsomal midazolam *N*-glucuronidation were 37.8 ± 3.6 μM and 276.0 ± 10.3 pmol/min/mg protein, respectively. An apparent K_m value similar to that obtained with human liver microsomes was observed for *N*-glucuronidation by recombinant UGT1A4 (29.9 ± 2.4 μM) with a V_{max} value at 659.6 ± 19.0 pmol/min/mg protein (Table 7).

Midazolam metabolic studies using freshly isolated human hepatocytes in primary culture

The metabolism of midazolam was investigated in fresh human hepatocytes in primary culture. Based on preliminary results on the rate of biotransformation of midazolam (5 µM initial concentration) in the absence and the presence of ketoconazole (10 µM), kinetic studies were performed over 6 to 8 hours.

Figure 11 illustrates the variability and the extremes in ketoconazole effect on midazolam disappearance kinetics on two different human hepatocytes preparations. While midazolam clearance is significantly decreased in the presence of ketoconazole in preparation HTL190, there is almost no inhibitory effect observed in preparation HTL234.

The inhibitory effect of ketoconazole on midazolam clearance was evaluated on a set of 29 human hepatocyte preparations which showed that this inhibitory effect of ketoconazole was highly variable from one subject/preparation to another. The mean inhibition value calculated on midazolam clearance decrease was of 42 ± 25 % with a range from 0 to 75 %. (Figure 12)

In addition to the effect of ketoconazole on midazolam clearance, the inhibitory effect of ketoconazole on the formation of midazolam CYP3A4/5-mediated metabolites, *i.e.* 1'-hydroxy-midazolam (1'OH-MDZ) and its conjugate (Glu-1'-O-MDZ) form was further investigated. Data are illustrated in Figure 13 for two different human hepatocytes preparations. Results demonstrated that ketoconazole completely abolished the midazolam 1'-hydroxylation metabolic pathway.

In Figure 14 the effect of ketoconazole on the formation of CYP3A4/5-mediated metabolites of midazolam on a set of 18 human hepatocyte preparations is illustrated. The mean inhibition value calculated on the 1'-hydroxylation pathway metabolite formation rate was 98 ± 5 % with a range from 83 to 100 %.

Given that ketoconazole often did not fully inhibit midazolam clearance and also that midazolam showed the potential to be glucurono-conjugated directly with UDPGA, the

formation of the direct *N*-glucuronide (N-Glu) conjugate was further investigated in two human hepatocytes preparations (Figure 15).

In the absence of ketoconazole, the *N*-glucuronide formation represented a very minor metabolic pathway and confirmed the predominant contribution of CYP3A4/5 to the overall *in vitro* clearance of midazolam with the formation of 1'-Hydroxy-midazolam further conjugated with glucuronic acid.

However, in the presence of ketoconazole, the complete inhibition of CYP3A4/5 was observed but the *N*-glucuronide conjugate formation increased and accounted for almost all of the midazolam clearance in these conditions. The increase in *N*-glucuronidation under ketoconazole co-incubation conditions was demonstrated in all human hepatocytes preparations investigated.

Inhibition of MDZ N- glucuronidation by ketoconazole

Like oxidative metabolism, drug glucuronidation may be inhibited by the co-administration of other chemicals (Miners and Mackenzie, 1991). Since ketoconazole has been described to inhibit glucuronidation of several drugs (Satoh, et al., 2004; Yong, et al., 2005; Takeda, et al., 2006), the rate of direct *N*-glucuronidation of midazolam formation using human liver microsomes and human recombinant UGT1A4 in the presence of the inhibitor has been investigated (Figure 16).

For these experiments, using either human liver microsomes or *rh*UGT1A4, MDZ concentration was set to 30 µM, *i.e.* close to the observed K_m and, under these conditions, we observed no significant inhibition of direct midazolam *N*-glucuronidation rate in the presence of ketoconazole.

Discussion

When incubating midazolam, a well-known *in vitro* and *in vivo* CYP3A4/5 probe substrate, with human liver microsomes in the presence of UDPGA, we observed the formation of two *N*-glucuronide conjugates. Looking at midazolam structure, three distinct direct *N*-glucuronidation positions were plausible. It was confirmed by LC-MS/MS analysis that the peaks observed in HPLC were direct midazolam *N*-glucuronides since the MS^2 and MS^3 spectra of the metabolite peaks were consistent with the MS^2 spectrum of midazolam. Additional ^1H NMR characterization demonstrated that both conjugates were β-*N*-glucuronides of MDZ. Those studies also showed that, since the ^1H NMR spectra of both glucuronides were very close, both conjugates were probably conformers of the same β-*N*-glucuronide. Molecular modelling studies suggested that these conjugates could be involved in atropoisomerism equilibrium and determined the glucuronidation position on the methyl-imidazole moiety.

Moderate inter-individual variability in midazolam *N*-glucuronidation was observed among the ten human liver microsomes preparations used (at most 4.5-fold, n = 10). Further characterization studies using commercially available baculovirus-infected insect cells demonstrated that recombinant UGT1A4 was the single human UGT isoform able to glucuronidate midazolam among all the recombinant UGT isoforms available. K_m value determined with *rh*UGT1A4 was similar to that observed with human liver microsomes, 29.9 ± 2.4 µM *versus* 37.8 ± 3.6 µM, respectively. These results suggest that the major liver UGT isoform catalyzing midazolam direct glucuronidation is UGT1A4, in accordance with the results recently published by Zhu *et al*. (2007). Because of the comparable apparent K_m of UGT1A4 relative to the K_m value obtained in human liver microsomes, the contribution of UGT1A4 to midazolam clearance is subject to its relative abundance in tissues such as liver and gut.

Complementary studies were performed on fresh human hepatocytes in primary culture. The presence of the midazolam *N*-glucuronide was also evidenced in samples in control conditions as well as, and to a much greater extent, in the presence of the specific CYP3A4 inhibitor, ketoconazole. These observations suggest a metabolic shift phenomenon between the CYP3A4 1'-hydroxylation pathway and direct *N*-glucuronidation of midazolam evidenced in the presence of specific and complete CYP3A4 inhibition such as that exerted by ketoconazole.

Similar observations were also made when looking for midazolam *N*-glucuronidation in plasma samples of patients treated with midazolam and a potent proprietary CYP3A4/5 inhibitor. Like in human hepatocyte preparations, a large inter-subject variability was observed in glucuronidation efficiency *in vivo* (data not shown, further investigations are on going)

In the present study, an additional metabolic pathway to the well-known CYP3A4/5-mediated oxidative process of midazolam has been revealed. Indeed, a potential metabolic shift from midazolam 1'-hydroxylation to direct *N*-glucuronidation has been evidenced *in vitro* principally in the presence of ketoconazole. Those findings provide evidence that direct *N*-glucuronidation could play an important role in midazolam clearance *in vitro* as well as *in vivo*. The apparent K_m and V_{max} values obtained could result in quite high glucuronidation efficiency *in vivo.*

Thus, the results obtained in this study should be taken into account when trying to predict the magnitude of a DDI that could occur in patients under ketoconazole treatment. Indeed, the occurrence of midazolam direct *N*-glucuronidation could lead to a certain extent of under-estimation of the ketoconazole inhibitory effect at least *in vitro*, and maybe also *in vivo* since in the clinic, the magnitude of a DDI is mainly evaluated based on the midazolam exposure,

the fold increase in the presence of a CYP3A4 inhibitor and not on the decrease of the specific CYP3A4-mediated midazolam-1'-hydroxylation route.

Thus, particularly for patients exhibiting a large glucuronidation capacity *via* the midazolam direct *N*-glucuronidation pathway (most likely linked to a high UGT1A4 capacity), the overall increase in midazolam plasma exposure observed is a contribution of partial or total suppression of the midazolam 1'-hydroxylation pathway, and the partly compensating enhanced direct *N*-glucuronidation pathway.

Such findings could account, at least in part, for the large variability observed in the ketoconazole effect from one patient to another since they suggest that midazolam clearance would not be exclusively associated with CYP3A4/5. Indeed, inter-subject variability could not only be related to CYP3A4 variability but also to variability in *N*-glucuronidation (UGT1A4) capacity. For instance, *N*-glucuronidation could be an alternative metabolic pathway when poor CYP3A4 activity is shown. This means that, inter-subject variability in glucuronidation (Ehmer, et al., 2004) combined with inter-individual variability in CYP3A4 metabolism should be considered at this stage when using midazolam as an *in vitro* as well as *in vivo* probe for DDI studies.

Acknowledgements

The authors wish to thank Dr. J.-L. Reversat (Sanofi-Aventis, CAS, Montpellier) for expert molecular modelling work, Dr. E. Sultan (Sanofi-Aventis, GMPK, Montpellier) for kindly supplying human plasma samples and Dr. Chandra Natarajan (Sanofi-Aventis, DMPK-S, Bridgewater) for a careful reading of the document and its scientific expertise.

References

Bjornsson TD, Callaghan JT, Einolf HJ, Fischer V, Gan L, Grimm S, Kao J, King SP, Miwa G, Ni L, Kumar G, McLeod J, Obach RS, Roberts S, Roe A, Shah A, Snikeris F, Sullivan JT, Tweedie D, Vega JM, Walsh J and Wrighton SA (2003) The conduct of in vitro and in vivo drug-drug interaction studies: A pharmaceutical research and manufacturers of America (PhRMA) perspective. *Drug Metab Dispos* **31**:815-832.

Bourrié M, Meunier V, Berger Y and Fabre G (1996) Cytochrome P450 isoform inhibitors as a tool for the investigation of metabolic reactions catalyzed by human liver microsomes. *Journal of Pharmacology & Experimental Therapeutics 277(1):321-32*.

Campos MPA, Bergter L, De Paula e Silva C.H.T. and Seidl PR (1999) Internal rotation process in endo-cis-N-(o-tolyl)bicyclo[2.2.1]heptene-2.3-dicarboximide and its oxidation products. *Magn Reson Chem* **37**:317-321.

Chung E, Nafziger AN, Kazierad DJ and Bertino JS Jr (2006) Comparison of midazolam and simvastatin as cytochrome P450 3A probes. *Clin Pharmacol Ther* **79**: 350-61.

Dundee JW, Halliday NJ, Harper KW and Brogden RN (1984) Midazolam. A review of its pharmacological properties and therapeutic use. *Drugs 28(6):*519-43.

Ehmer U, Vogel A, Schutte JK, Krone B, Manns MP and Strassburg CP (2004) Variation of Hepatic Glucuronidation: Novel Functional Polymorphisms of the UDP-Glucuronosyltransferase UGT1A4. *Hepatology 39(4) pp 970-977*.

Fabre G, Rahmani R, Placidi M, Combalbert J, Covo J, Cano JP, Coulange C, Ducros M and Rampal M (1988a) Characterization of midazolam metabolism using human hepatic microsomal fractions and hepatocytes in suspension obtained by perfusing whole human livers. *Biochemical Pharmacology 37(22):4389-97*.

Fabre G, Crevat-Pisano P, Dragna S, Covo J, Barra Y and Cano JP (1988b) Involvement of the macrolide antibiotic inducible cytochrome P-450 LM3c in the metabolism of midazolam by microsomal fractions prepared from rabbit liver. *Biochemical Pharmacology 37(10):1947-53*.

Galetin A, Ito K, Hallifax D and Houston JB (2005) CYP3A4 Substrate selection and substitution in the prediction of potential drug-drug interactions. *J Pharmacol Exp Ther* **314**:180-190.

Gascon MP and Dayer P (1991) In vitro forecasting of drugs which may interfere with the biotransformation of midazolam. *European Journal of Clinical Pharmacology* **41**:573-578.

Ghosal A, Satoh H, Thomas PE, Bush E and Moore D (1996) Inhibition and kinetics of cytochrome P4503A activity in microsomes from rat, human, and cdna-expressed human cytochrome P450. *Drug Metab Dispos* **24**:940-947.

Gorski JC, Hall SD, Jones DR, VandenBranden M and Wrighton SA (1994) Regioselective biotransformation of midazolam by members of the human cytochrome P450 3A (CYP3A) subfamily. *Biochemical Pharmacology 47(9):1643-53*.

Guengerich FP (1995) Human cytochrome P450 enzymes, in *Cytochrome P450*.

Heizmann P and Ziegler WH (1981) Excretion and metabolism of 14C-midazolam in humans following oral dosing. *Arzneimittel-Forschung 31(12a):2220-3*.

Hosea NA, Miller GP and Guengerich FP (2000) Elucidation of distinct ligand binding sites for Cytochrome P450 3A4. *Biochemistry* **39**:5929-5939.

Ismail IM, Dear GJ, Roberts AD, Plumb RS, Ayrton J, Sweatman BC and Bowers GD (2002) N-O glucuronidation: a major human metabolic pathway in the elimination of two novel anti-convulsant drug candidates. *Xenobiotica* **32**:29-43.

Isom HC and Georgoff I (1984) Quantitative assay for albumin-producing liver cells after simian virus 40 transformation of rat hepatocytes maintained in chemically defined medium. *Proceedings of the National Academy of Sciences of the United States of America 81(20):6378-82*.

Kemp DC, Fan PW and Stevens JC (2002) Characterization of raloxifene glucuronidation in vitro: Contribution of intestinal metabolism to presystemic clearance. *Drug Metab Dispos* **30**:694-700.

Kronbach T, Mathys D, Umeno M, Gonzalez FJ and Meyer UA (1989) Oxidation of midazolam and triazolam by human liver cytochrome P450IIIA4. *Mol Pharmacol* **36**:89-96.

Kuehl P, Zhang J, Lin Y, Lamba J, Assem M, Schuetz J, Watkins PB, Daly A, Wrighton SA, Hall SD, Maurel P, Relling M, Brimer C, Yasuda K, Venkataramanan R, Strom S, Thummel K, Boguski MS and Schuetz E (2001) Sequence diversity in CYP3A promoters and characterization of the genetic basis of polymorphic CYP3A5 expression. *Nat Genet* **27**:383-391.

Lam Y, Ereshefsky L, Alfaro C and Miller M (1999) In vivo inhibition of midazolam disposition by ketoconazole and fluoxetine, and comparison to in vitro prediction. *Clin Pharmacol Ther* **65:** 143.

Lam Y, Alfaro C, Ereshefsky L and Miller M (2003) Pharmacokinetic and pharmacodynamic interactions of oral midazolam with ketoconazole, fluoxetine, fluvoxamine, and nefazodone. *J Clin Pharmacol* **43:** 1274-1282.

Lee JI, Chaves-Gnecco D, Amico JA, Kroboth PD,Wilson JW and Frye RF (2002) Application of semisimultaneous midazolam administration for hepatic and intestinal cytochrome P450 3A phenotyping. *Clin Pharmacol Ther* **72:** 718-728.
Maenpaa J, Hall SD and Ring BJ (1998) Human cytochrome P450 3A (CYP3A) mediated midazolam metabolism: the effect of assay conditions and regioselective stimulation by alpha-naphtoflavone, terfenadine and testosterone. *Pharmacogenetics* **8**:137-155.

Miners JO and Mackenzie PI (1991) Drug glucuronidation in humans. *Pharmacology & Therapeutics* **51**:347-369.

Olkkola KT, Backman JT and Neuvonen PJ (1994) Midazolam should be avoided in patients receiving the systemic antimycotics ketoconazole or itraconazole. *Clin Pharmacol Ther* **55:** 481-485

OMURA T and SATO R (1964) The carbon monoxide-binding pigment of liver microsomes. I. Evidence for its hemoprotein nature. *Journal of Biological Chemistry 239:2370-8*.

Pollard HB, Menard R, Brandt HA, Pazoles CJ, Creutz CE and Ramu A (1978) Application of Bradford's protein assay to adrenal gland subcellular fractions. *Analytical Biochemistry 86(2):761-3*.

Reves JG, Fragen RJ, Vinik HR and Greenblatt DJ (1985) Midazolam: pharamcology and uses. *Anesthesiology* **62**:310-324.

Satoh T, Tomikawa Y, Takanashi K, Ito S and Yoshizawa I (2004) Studies on the interaction between drugs and estrogen.III. Inhibitory effects of 29 drugs reported to induce gynecomastia on the glucuronidation of estradiol. *Biological & Pharmaceutical Bulletin* **27**:1844-1849.

Schantl JG (1995) Synthetic, structural, reactive and biological aspects of novel tetraazabicyclooctanes. *Farmaco 50(6) pp 379-394*.

Siddle DW, Faithfull L, Gleave M, Wright P, Lindsay N and Khol C (2003) Midazolam is metabolized by UGT1A4 in human hepatocytes and hepatic microsomes. *Drug Metabolism Reviews* **35**:55.

Srivastav KK, Verma AK and Verma SM (1993) Torsional barriers about N-C(aryl) bond and atropoisomerism: A ^{1}H NMR study. *Indian J Chem* **32B**:1143-1148.

Takeda S, Kitajima Y, Ishii Y, Nishimura Y, Mackenzie PI, Oguri K and Yamada H (2006) Inhibition of UDP-glucuronosyltransferase 2B7-catalyzed morphine glucuronidation by ketoconazole: dual mechanisms involving a novel noncompetitive mode. *Drug Metab Dispos* **34**:1277-1282.

Thummel KE and Wilkinson GR (1998) In vitro and in vivo drug interactions involving human CYP3A. *Annual Review of Pharmacology and Toxicology* **38**:389-430.

Tsunoda SM, Velez RL and Greenblatt DJ (1999) Ketoconazole (K) inhibition of intestinal and hepatic cytochrome P450 3A4 (CYP3A4) activity using midazolam (M) as an in vivo probe. *Clin Pharmacol Ther* **65:** 172.

Voitenko ZV, Pokholenko AA, Shkarov OO, Kovtunenko VA and Babichev FS (2002) Cycloaddition in condensed isoindoles.2*. Method for obtaining new derivatives of 2-phenylpyridine. *Chem Heter Comp* **38**:190-196.

von Moltke LL, Greenblatt DJ, Schmider J, Duan SX, Wright CE, Harmatz JS and Shader RI (1996) Midazolam hydroxylation by human liver microsomes in vitro: inhibition by fluoxetine, norfluoxetine, and by azole antifungal agents. *J Clin Pharmacol* **36**:783-791.

Wang RW, Newton DJ, Liu N, Atkins WM and Lu AYH (2000) Human cytochrome P-450 3A4: In vitro drug-drug interaction patterns are substrate-dependent. *Drug Metab Dispos* **28**:360-366.

Wrighton SA and Ring BJ (1994) Inhibition of human CYP3A catalyzed 1'-hydroxymidazolam formation by ketoconazole, nifedipine, erythromycin, cimetidine, and nizatidine. *Pharmaceutical Research* **11**:921-924.

Yong WP, Ramirez J, Innocenti F and Ratain MJ (2005) Effects of ketoconazole on glucuronidation by UDP-glucuronosyltransferase enzymes. *Clin Cancer Res* **11**:6699-6704.

Zhu B, Bush D, Doss GA, Vincent SH, Franklin RB and Xu S (2007) Characterization of 1'-hydroxymidazolam glucuronidation in human liver microsomes. *Drug Metab Dispos* (Epub ahead of print DOI: 10.1124/dmd.107.017962).

Footnotes

Address correspondence to: Gérard FABRE, DMPK-S department, Sanofi-aventis Recherche 34184 Montpellier, France. E-mail: gerard.fabre@sanofi-aventis.com.

List of figures

Figure 1: Chemical structure of Midazolam

Figure 2: Representative HPLC-UV chromatograms of midazolam and midazolam-N-glucuronides (M1 and M2) formed after incubation of 100 µM midazolam with 1 mg/mL microsomes in the presence of 3 mM UDPGA

Figure 3: Representative MS^n mass spectra of midazolam and midazolam *N*-glucuronides (M1 and M2)
(a) Mass spectrum of midazolam; (b) Mass spectrum of metabolite M1; (c) Mass spectrum of metabolite M2; (d) MS^2 mass spectrum of metabolite M1; (e) MS^2 mass spectrum of metabolite M2; (f) MS^3 mass spectrum of metabolite M1; (g) MS^3 mass spectrum of metabolite M2; (h) MS^2 mass spectrum of midazolam

Figure 4: ^1H 1D NMR M_1/M_2 mixture, glucuronide signals (ON-LINE NMR, 500 MHz)

Figure 5: ^1H 1D NMR M1/M2 mixture, aromatic region (OFF-LINE NMR, 600 MHz)

Figure 6: Structure of midazolam *N*-glucuronide

Figure 7: Proposed metabolic pathways of midazolam in humans

Figure 8: Inter-individual variability in Midazolam *N*-glucuronide formation rate in human liver microsomes.
Human liver microsomal fractions were incubated for 60 minutes with 100 µM Midazolam. At the end of the incubation, proteins were precipitated and Midazolam *N*-glucuronide quantified by HPLC-UV relative to a standard Midazolam reference curve. The rate of Midazolam *N*-glucuronide formation was determined (Data represent mean of a triplicate experiment).

Figure 9: Formation of Midazolam *N*-glucuronide in human recombinant UGT isozymes.

Human recombinant UGT microsomal fractions were incubated for 60 minutes with 100 µM Midazolam and 3 mM UDPGA. At the end of the incubation, proteins were precipitated and Midazolam-*N*-glucuronide quantified by HPLC-UV relative to a standard Midazolam reference curve. The rate of Midazolam *N*-glucuronide formation was determined. (Data represent mean of a triplicate experiment).

Figure 10: Midazolam concentration-dependent metabolite formation with human liver microsomes from donor HTL19 (A) or with UGT1A4 (B).
Human liver microsomes or cDNA expressed UGT1A4 microsomes were incubated for 60 minutes at 37°C in the presence of UDPGA with various concentrations of Midazolam. At the end of the incubation, proteins were precipitated and Midazolam *N*-glucuronide quantified by HPLC-UV relative to a standard Midazolam reference curve. The initial rate of Midazolam N-glucuronide formation was determined for each concentration and plotted in order to determine K_m and V_{max}. The units are µM for K_m and pmol/min/mg protein for V_{max} (Data represent mean of a triplicate experiment).

Figure 11: Midazolam disappearance kinetics with and without ketoconazole in human hepatocytes preparations HTL190 (A) and HTL234 (B).

Figure 12: Midazolam clearance in mL/h/10^6 cells in human hepatocytes in the absence or the presence of ketoconazole (n = 29 donors).
[A: Mean value of n = 29 human hepatocytes preparations, *** significantly different from control which was determined in the absence of inhibitor ($p < 0.0001$) ;
B: Individual plotted values of n = 29 human hepatocytes preparations (•) ; mean value (□)]

Figure 13: Kinetics of midazolam disappearance and metabolites formation in the absence or the presence of ketoconazole in human hepatocytes preparations HTL203 (A) and HTL233 (B).

Figure 14: CYP3A4/5-mediated 1'-OH-MDZ (+ subsequent MDZ-1'-O-glucuronide) metabolites formation rate in nmol/h/10^6 cells in human hepatocytes in the absence or the presence of ketoconazole.

[A: Mean value of n = 18 human hepatocytes preparations, *** significantly different from control which was determined in the absence of inhibitor ($p < 0.0001$)
B: Individual plotted values of n = 18 human hepatocytes preparations (•) ; mean value (□)]

Figure 15: Kinetics of midazolam disappearance and metabolites formation in the absence or the presence of ketoconazole in human hepatocytes preparations HTL200 (A) and HTL202 (B).

Figure 16: Formation of Midazolam *N*-glucuronide with human liver microsomes from three donors and cDNA-expressed UGT1A4 in the absence and the presence of 1.5 or 10 µM ketoconazole.
Microsomes from donors FH49, HTL20 and HTL19 and cDNA-expressed UGT1A4 were incubated for 60 minutes at 37 °C with 30 µM midazolam. At the end of the incubation, proteins were precipitated and Midazolam *N*-glucuronide quantified by HPLC-UV relative to a standard Midazolam reference curve. The rate of Midazolam *N*-glucuronide formation was determined (Data represent mean of a triplicate experiment).

Tables

Table 1: CYP3A4 inhibitor ketoconazole with midazolam used as probe substrate in healthy volunteers

Ketoconazole dosage regimen	***Midazolam dosage regimen***	***Fold elevation in Midazolam exposure***	***Reference***
400 mg q.d. x 4 days	7.5 mg *p.o.*	16	Olkkola, et al., 1994
3 doses of 200 mg	6 mg *p.o.*	16	Tsunoda, et al., 1999
3 doses of 200 mg	2 mg *i.v.*	5	Tsunoda, et al., 1999
200 mg q.d. x 11 days	Not specified	8.7	Lam, et al., 1999
200 mg given simultaneously	2 mg *p.o.*	6.2	Olkkola, et al., 1994
200 mg given before	2 mg *p.o.*	5	Olkkola, et al., 1994
3 doses of 200 mg	5 mg *p.o.*	5	Lee, et al., 2002
200 mg q.d. x 12 days	10 mg *p.o.*	7	Lam, et al., 2003
400 mg q.d. x 10 days	5.5 mg *p.o.*	10	Chung, et al., 2006

DMD Fast Forward. Published on February 6, 2008 as DOI: 10.1124/dmd.107.019539
This article has not been copyedited and formatted. The final version may differ from this version.

Table 2: Examples of recommended in vitro probe substrates, inhibitors and inducers for CYP3A4 (adapted from FDA guidance, September 2006)

	Substrates		**Inhibitors**		**Inducers**	
P450	Preferred (K_m in µM)	Acceptable (K_m in µM)	Preferred (K_i in µM)	Acceptable (K_i in µM)	Preferred (recommended conc. in µM)	Acceptable (recommended conc. in µM)
3A4	Midazolam (1-14) Testosterone (52-94)	Nifedipine (5.1-47) Dextrometorphan (133-710) Triazolam (234) Terfenadine (15) Erythromycin (33-88)	Ketoconazole (0.0037-0.18) Itraconazole (0.27, 2.3)	Verapamil (10, 24) Troleandomycin (17)	Rifampin (10-50)	Phenobarbital (100-2000) Phenytoin (50) Rifapentine (50) Dexamethasone (4)

Table 3: Preferred in vivo CYP3A4 probe substrates, inhibitors and inducers (adapted from FDA guidance, September 2006)

P450	Substrates	Inhibitors	Inducers
3A4	Midazolam Buspirone Felodipine Simvastatin Lovastatin Eletriptan Sildenafil Triazolam	Ketoconazole Nefazodone Nelfinavir Ritonavir Saquinavir Telithromycin Atazanavir Clarithromycin Indinavir Itraconazole	Rifampin Carbamazepin

Table 4: Demographic information for donors used for liver microsomes preparation

Donor	Gender	Age	Cause of death
FH1	M	25	Head Injury (Traffic accident)
FH6	F	20	Autolysis (Gun Shot)
FH49	M	N.A.	N.A.
HL23	M	26	Head Injury (Traffic accident)
HL31	M	36	N.A.
HL32	M	32	N.A.
HTL19	F	61	Colon adenocarcinoma
HTL20	N.A.	N.A.	N.A.
HTL22	F	56	N.A.
HTL49	M	51	Colon adenocarcinoma

N.A. : Not available

DMD Fast Forward. Published on February 6, 2008 as DOI: 10.1124/dmd.107.019539
This article has not been copyedited and formatted. The final version may differ from this version.

Table 5: Demographic information for donors used for human hepatocytes preparations

Donor	Gender	Age	Cause of death
HTL-156	N.A.	N.A.	N.A.
HTL-157	N.A.	N.A.	N.A.
HTL-164	F	55	Colon adenocarcinoma
HTL-167	M	53	Colon adenocarcinoma
HTL-168	F	72	Carcinome
HTL-170	M	N.A.	Healthy
HTL-172	M	N.A.	Colon adenocarcinoma
HTL-176	M	57	Islet cell carcinoma
HTL-177	M	75	N.A.
HTL-181	F	72	Ovarian tumor
HTL-187	M	67	Colon adenocarcinoma
HTL-188	M	48	Renal tumor
HTL-189	M	71	Colon adenocarcinoma
HTL-190	N.A.	N.A.	N.A.
HTL-191	N.A.	N.A.	N.A.
HTL-192	F	65	Colon adenocarcinoma
HTL-193	M	54	Stroke CVA
HTL-194	F	61	Gall-bladder tumor
HTL-195	F	73	Colon adenocarcinoma
HTL-196	M	17	Traffic accident
HTL-197	F	60	N.A.
HTL-198	F	13	Encephalitis
HTL-199	N.A.	N.A.	N.A.
HTL-200	M	42	Caroli’s disease
HTL-201	M	71	Colon adenocarcinoma
HTL-202	M	72	Colon adenocarcinoma
HTL-203	M	69	Colon adenocarcinoma
HTL-233	F	55	Pancreas tumor
HTL-234	F	55	N.A.

N.A. : Not available

DMD Fast Forward. Published on February 6, 2008 as DOI: 10.1124/dmd.107.019539
This article has not been copyedited and formatted. The final version may differ from this version.

Table 6: ^{1}H and ^{13}C assignments for midazolam, ^{1}H assignments for M1 and M2.

(OFF-LINE NMR, DMSO-D_6, 600 MHz)

	Chemical shifts (ppm)		
	Midazolam		M1/M2 metabolites
Atom	^{1}H	^{13}C	^{1}H
4	5.20/4.18	43.3	5.23/4.22 and 5.22/4.21
16	7.24	115.8	7.24 / 7.24
15	7.56	132.1	7.57 / 7.57
14	7.31	124.3	7.32 / 7.31
13	7.60	130.9	7.64 / 7.61
7	7.38	129.2	7.43 / 7.40
9	7.91	131.1	7.93 / 7.90
10	7.98	126.7	8.00 / 7.95
3	**7.74**	113.4	**8.08 / 8.05**
12	**2.75**	12.1	**2.86 / 2.85**
17			5.50[a] / 5.46[a]
18			3.61[a] / 3.61[a]
19			3.54[a] / 3.52[a]
20			3.61[a] / 3.61[a]
21			4.1[a] / 4.1[a]

[a] In Acetonitrile-D_3, ON- LINE NMR, 500 MHz

Bold: main differences between midazolam and M1/M2 metabolites chemical shifts

Table 7: Enzyme kinetic parameters of Midazolam *N*-glucuronide in human liver microsomes HTL19 and recombinant UGT1A4.

	K_m (µM)	V_{max} (pmol/min/mg protein)
HTL19	37.8 ± 3.6	276.0 ± 10.3
***rh*UGT1A4**	29.9 ± 2.4	659 .6 ± 19.0

(The kinetic parameters were calculated with GraFit v 5 Sofware)

DMD Fast Forward. Published on February 6, 2008 as DOI: 10.1124/dmd.107.019539

Figure 1

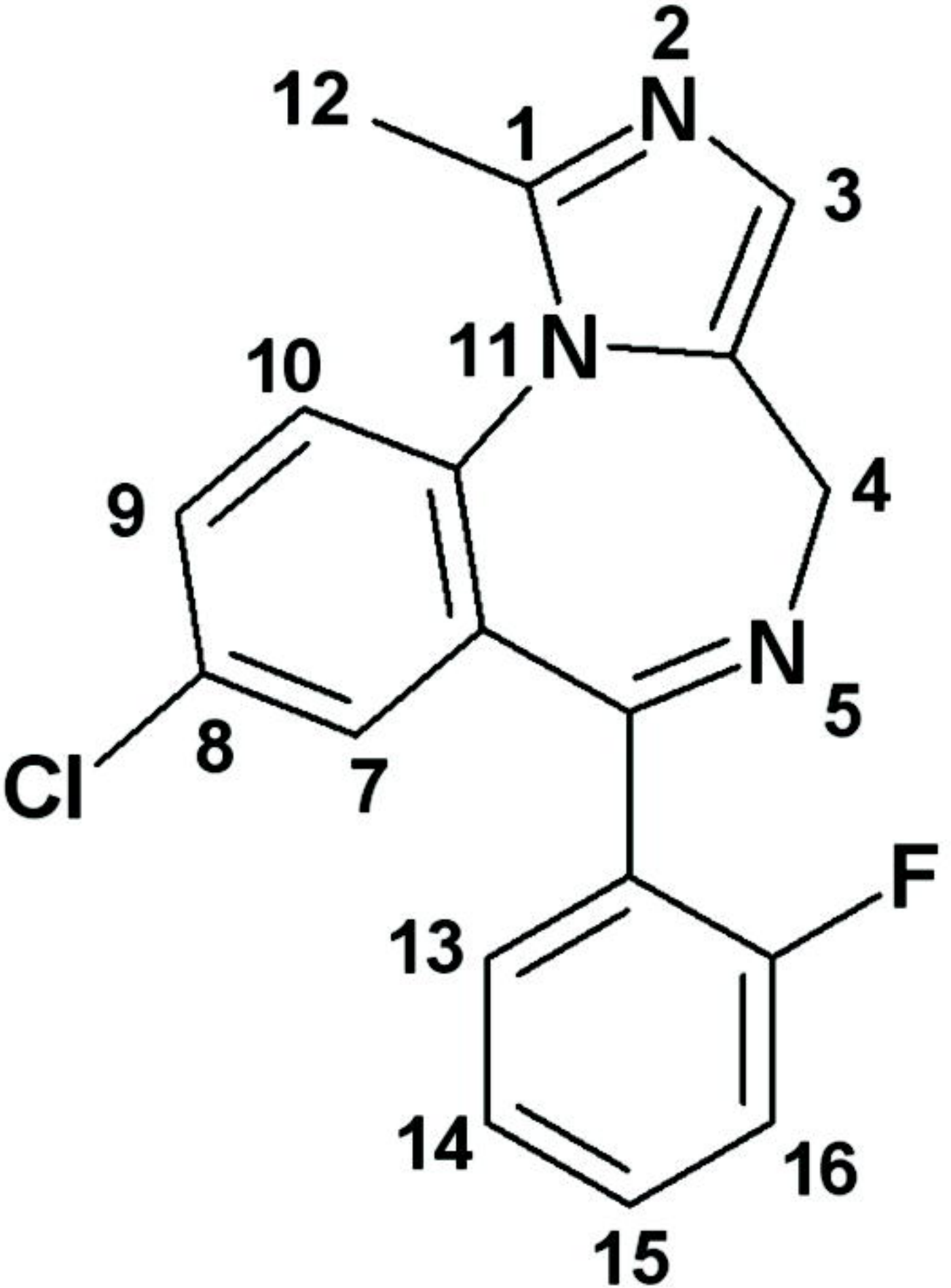

DMD Fast Forward. Published on February 6, 2008 as DOI: 10.1124/dmd.107.019539

Figure 2

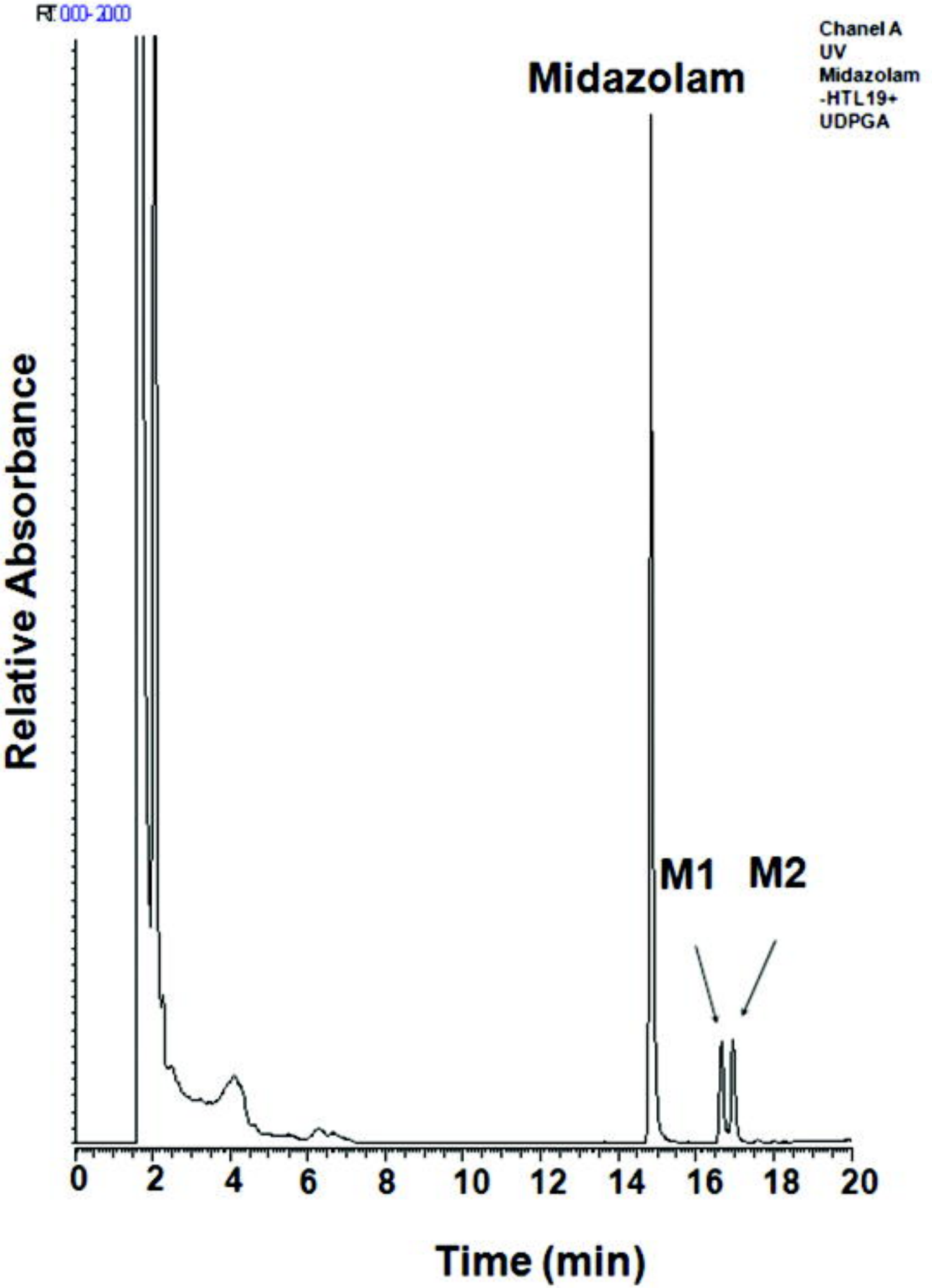

Figure 3a

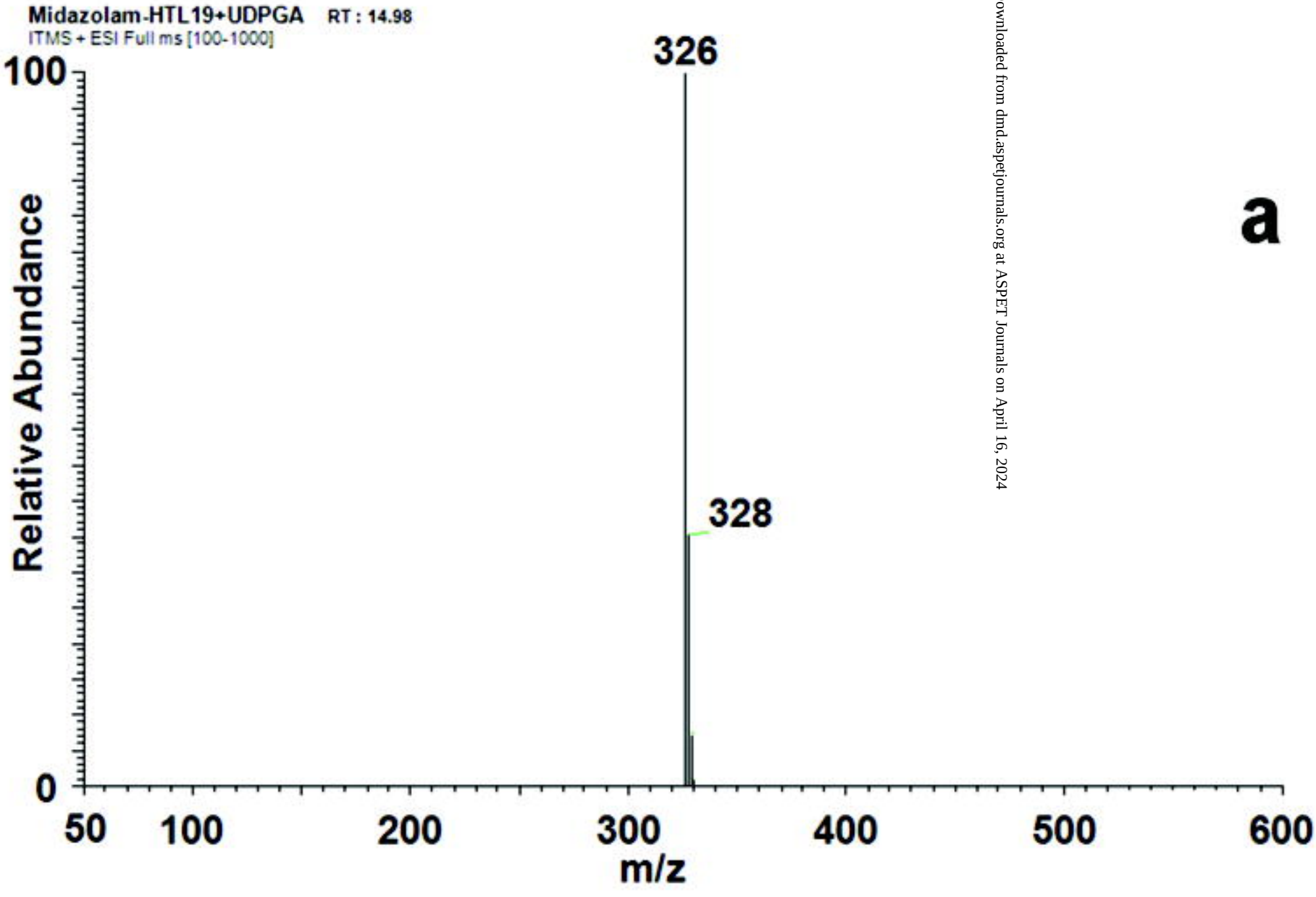

Figure 3b

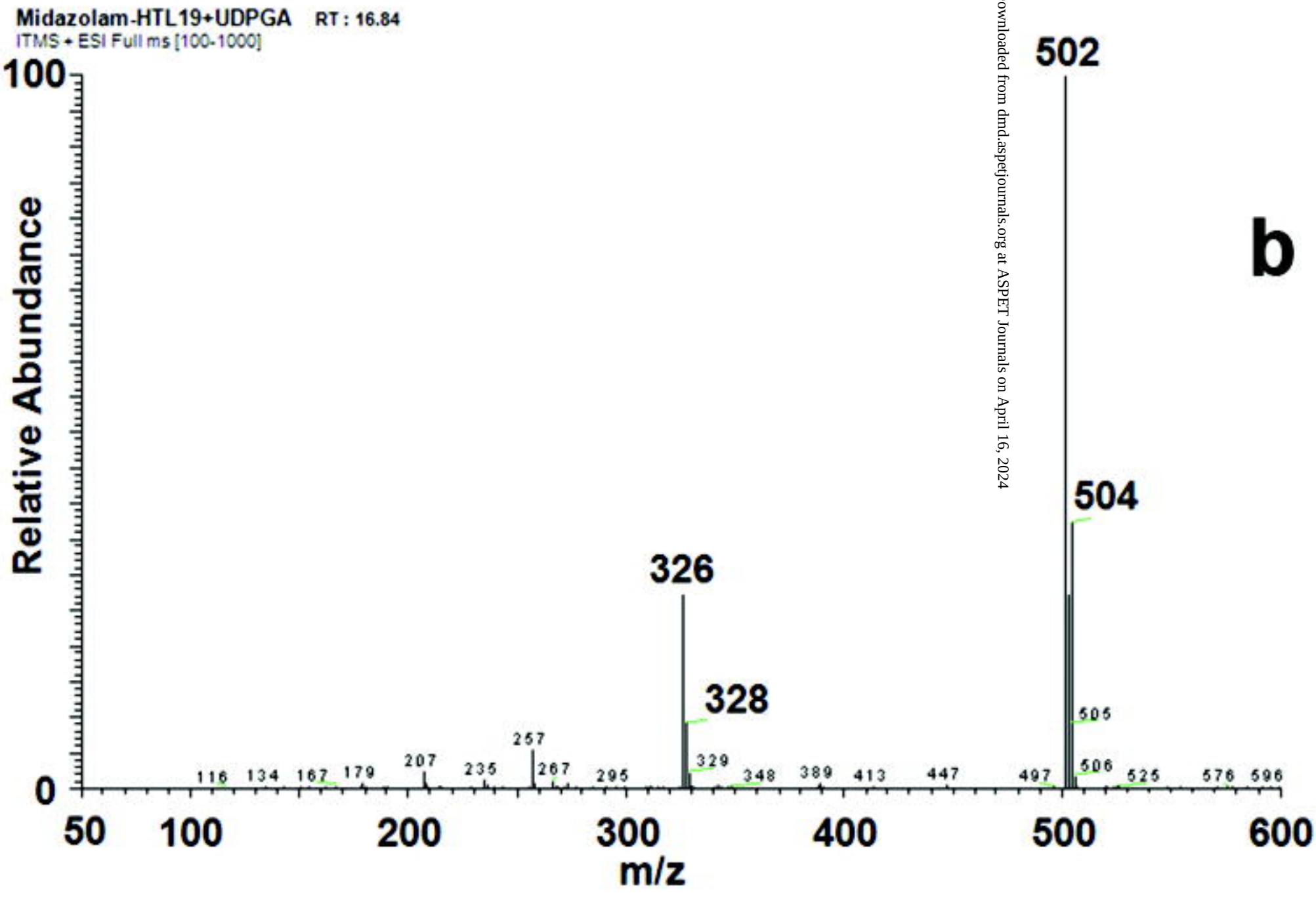

Figure 3c

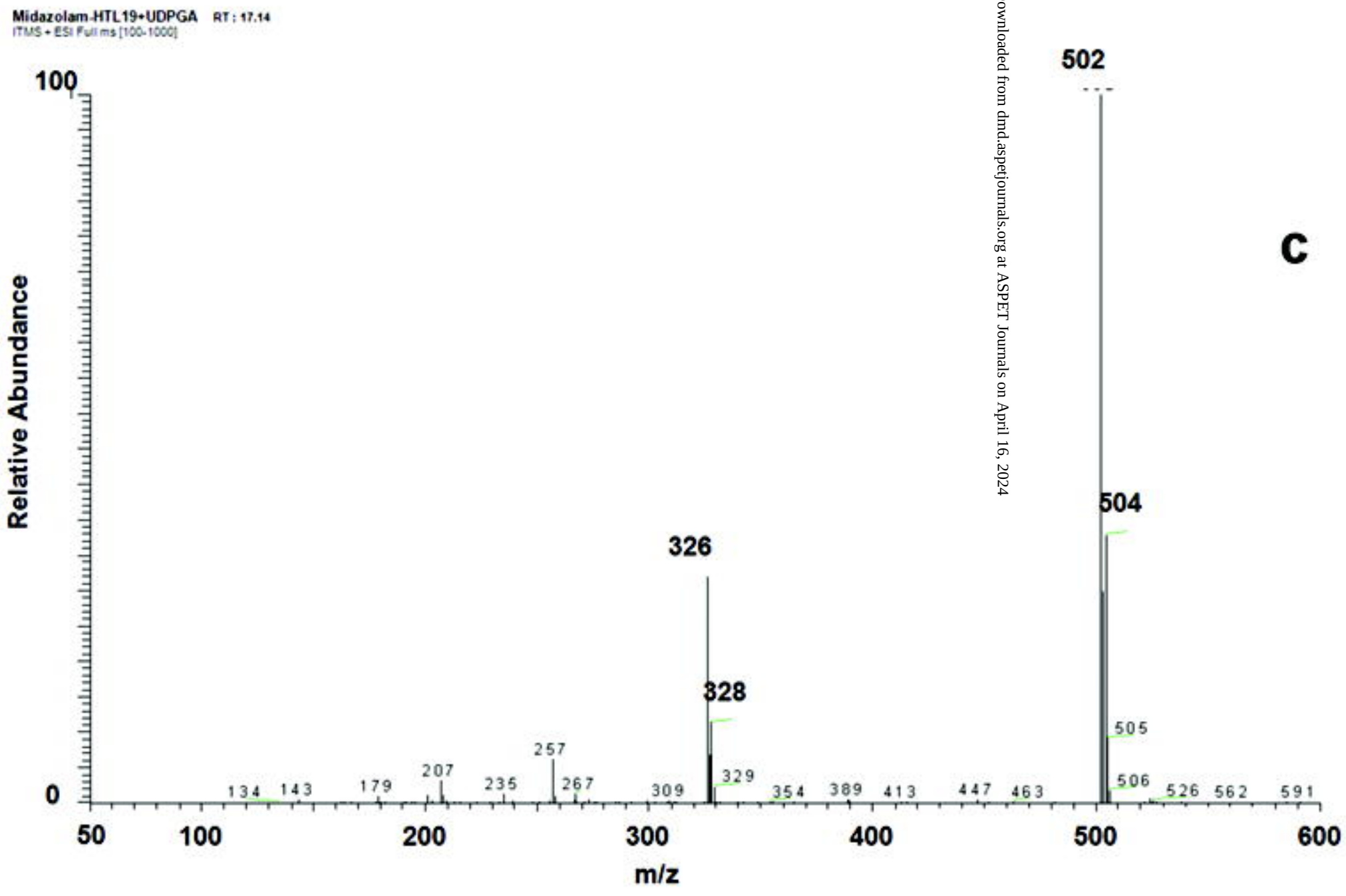

Figure 3d

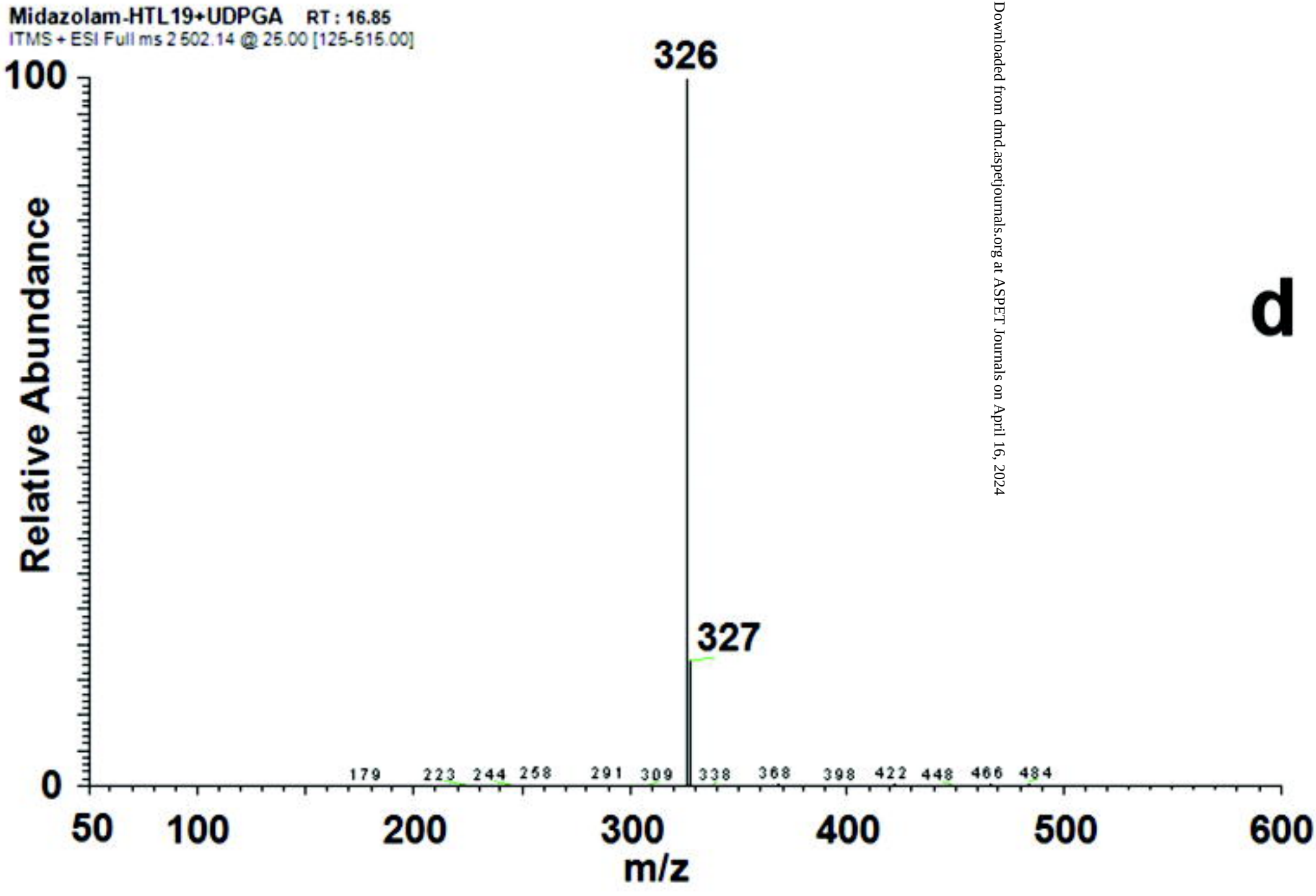

Figure 3e

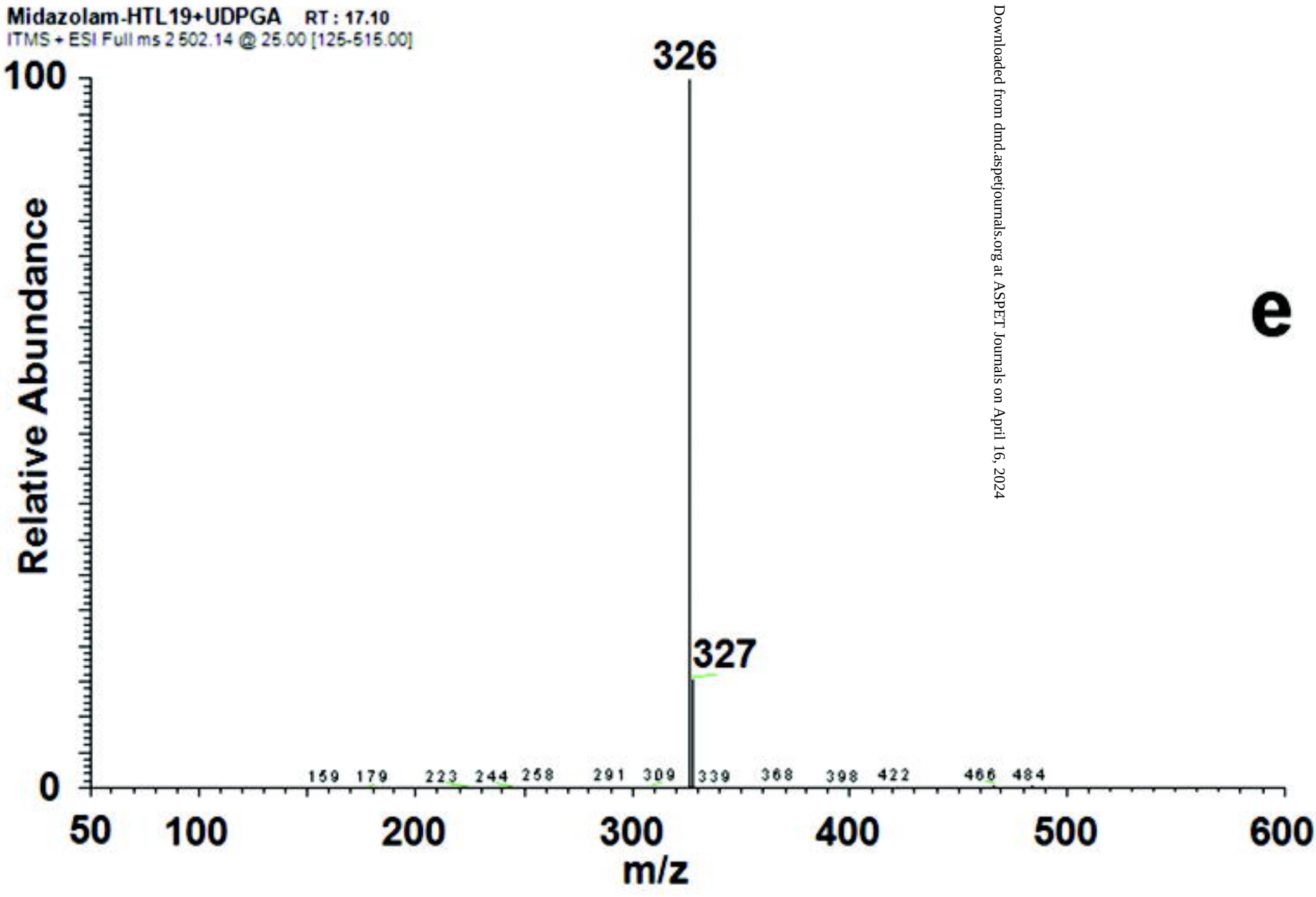

Figure 3f

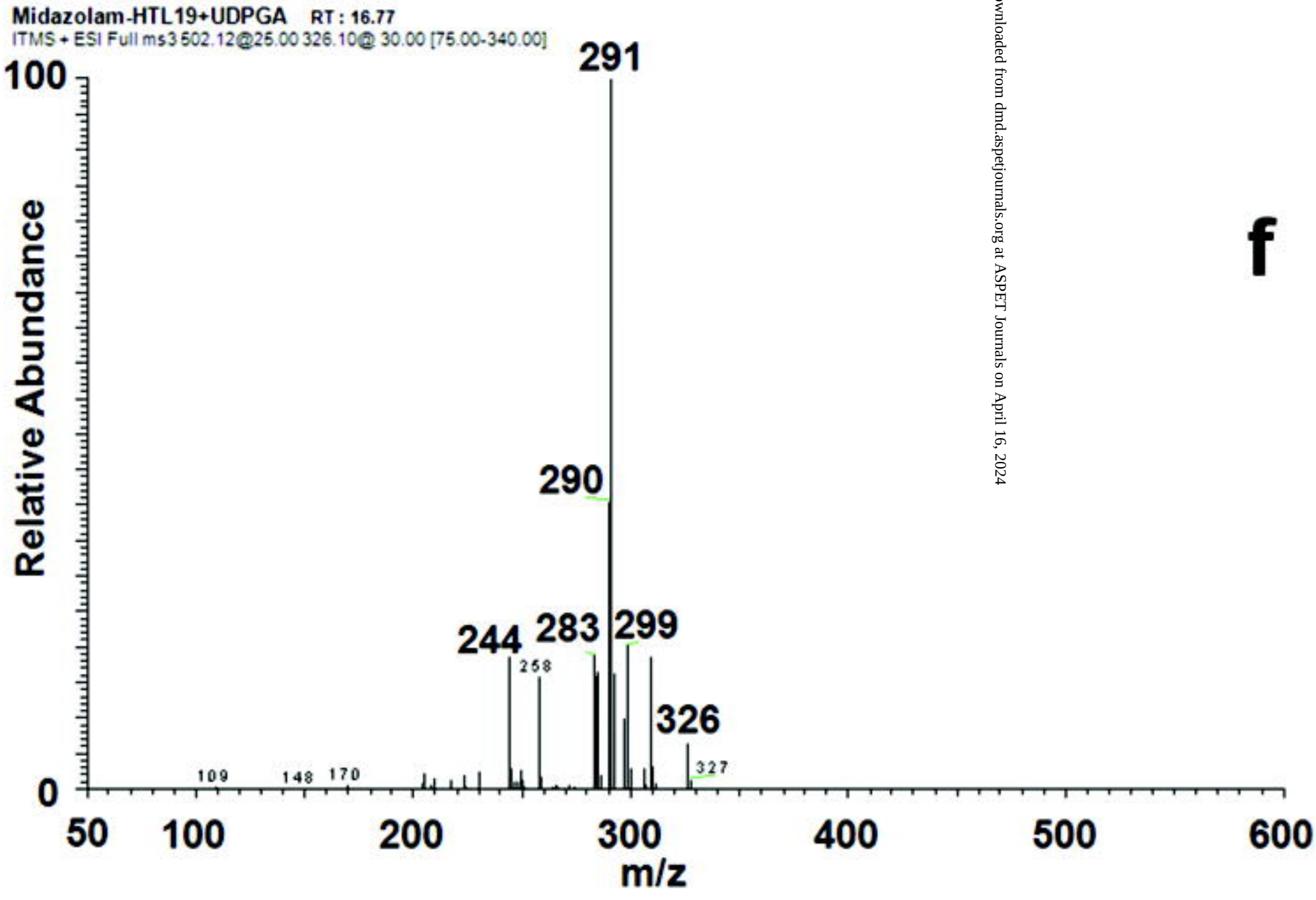

Figure 3g

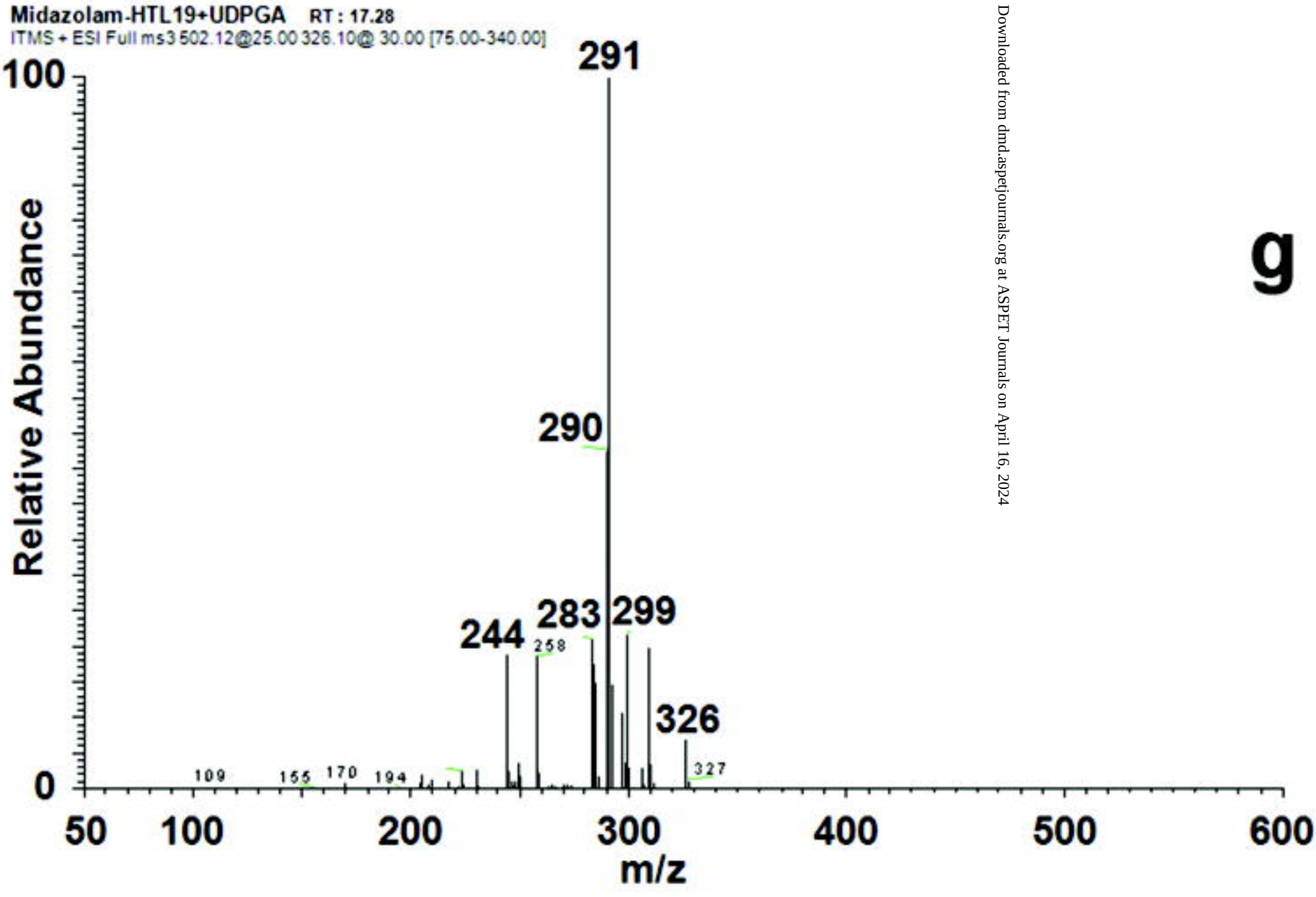

Figure 3h

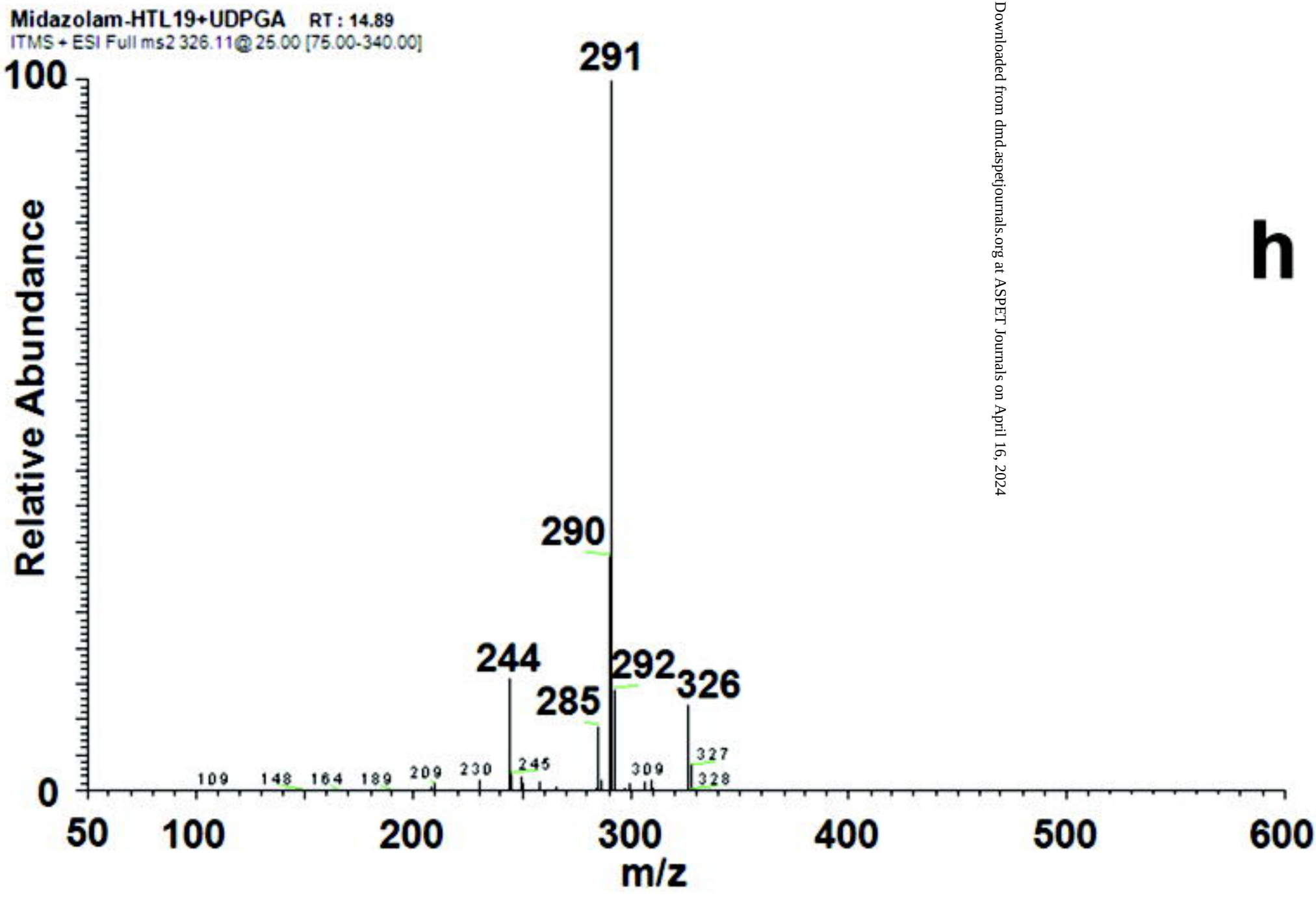

Figure 4

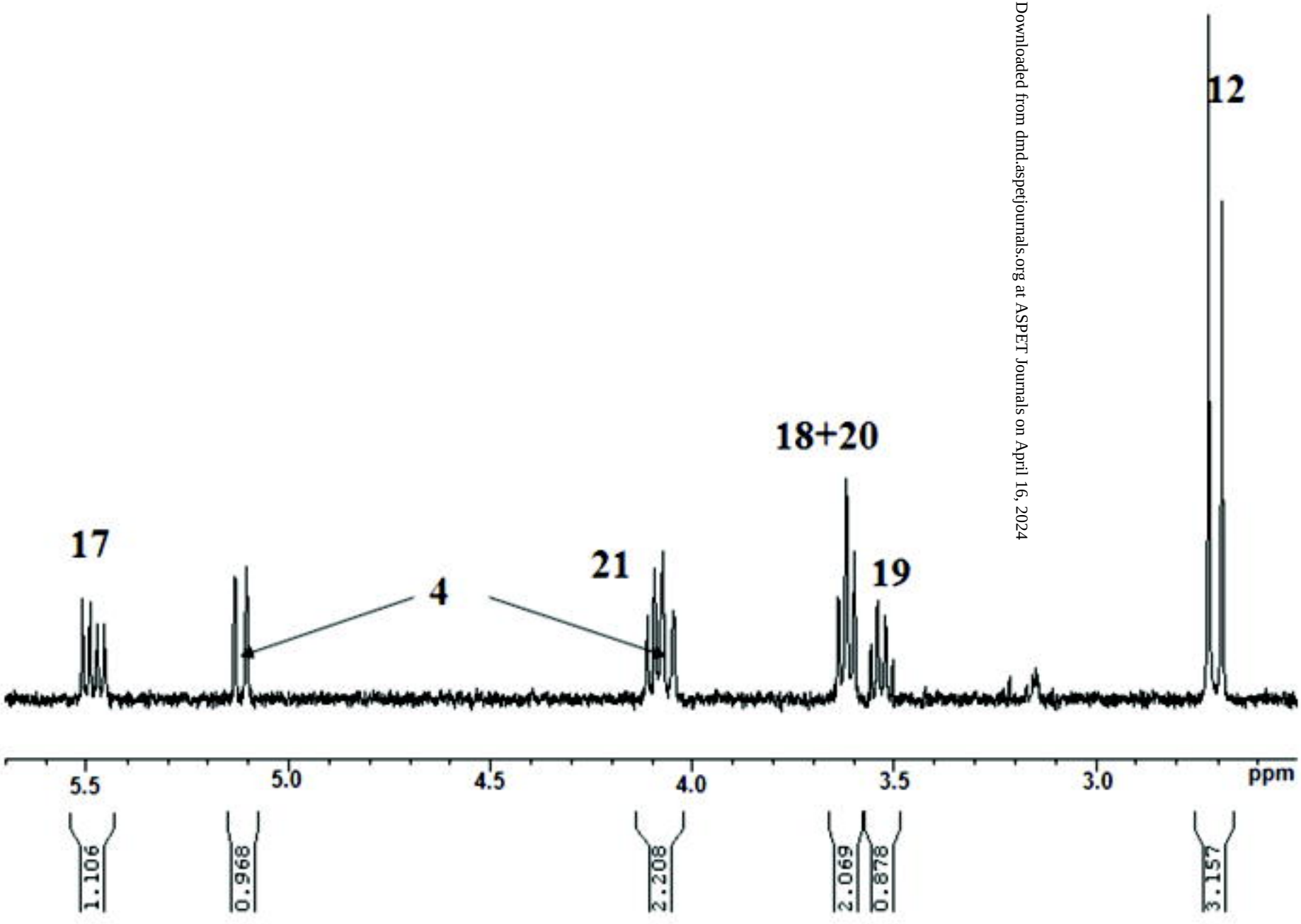

Figure 5

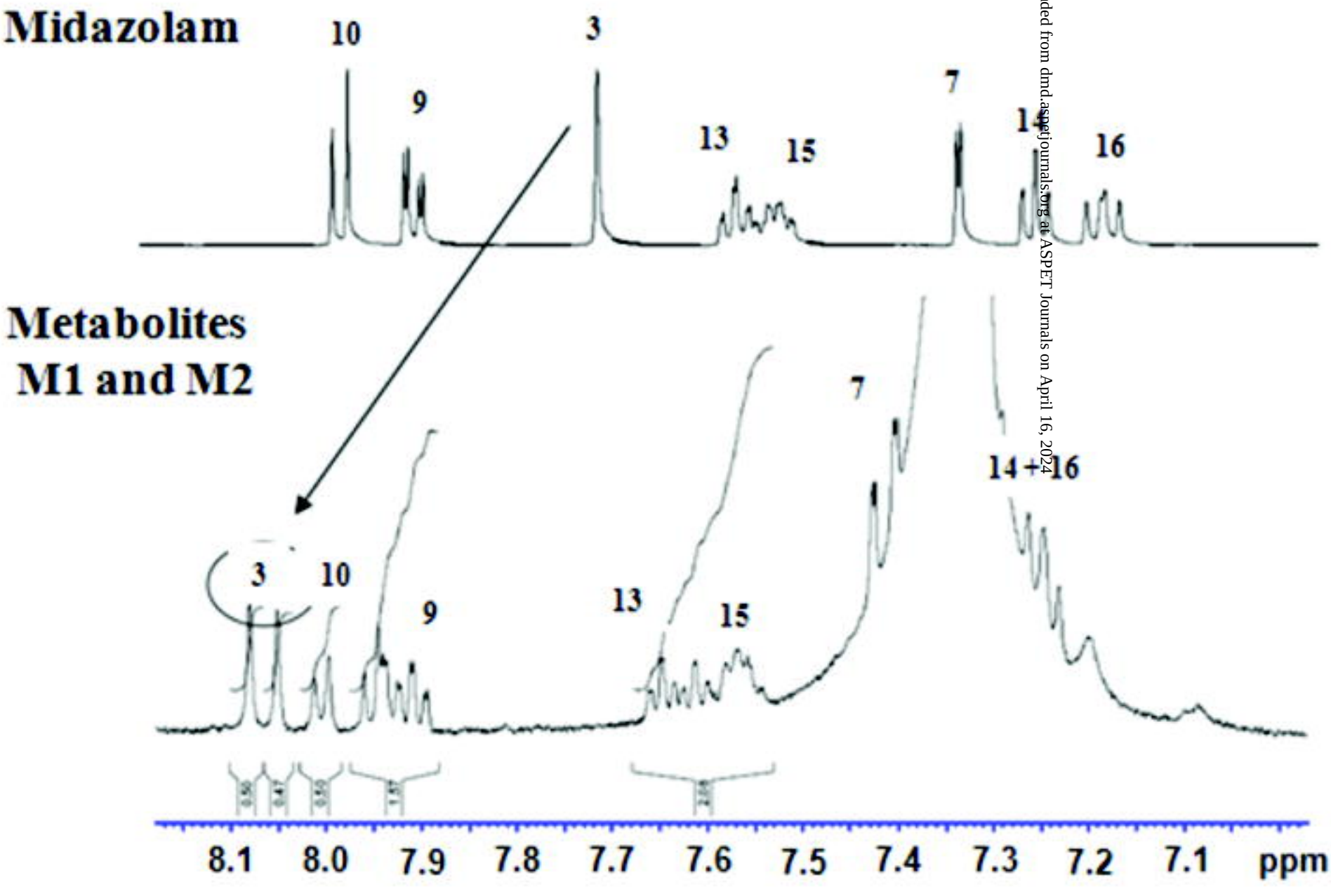

DMD Fast Forward. Published on February 6, 2008 as DOI: 10.1124/dmd.107.019539

Figure 6

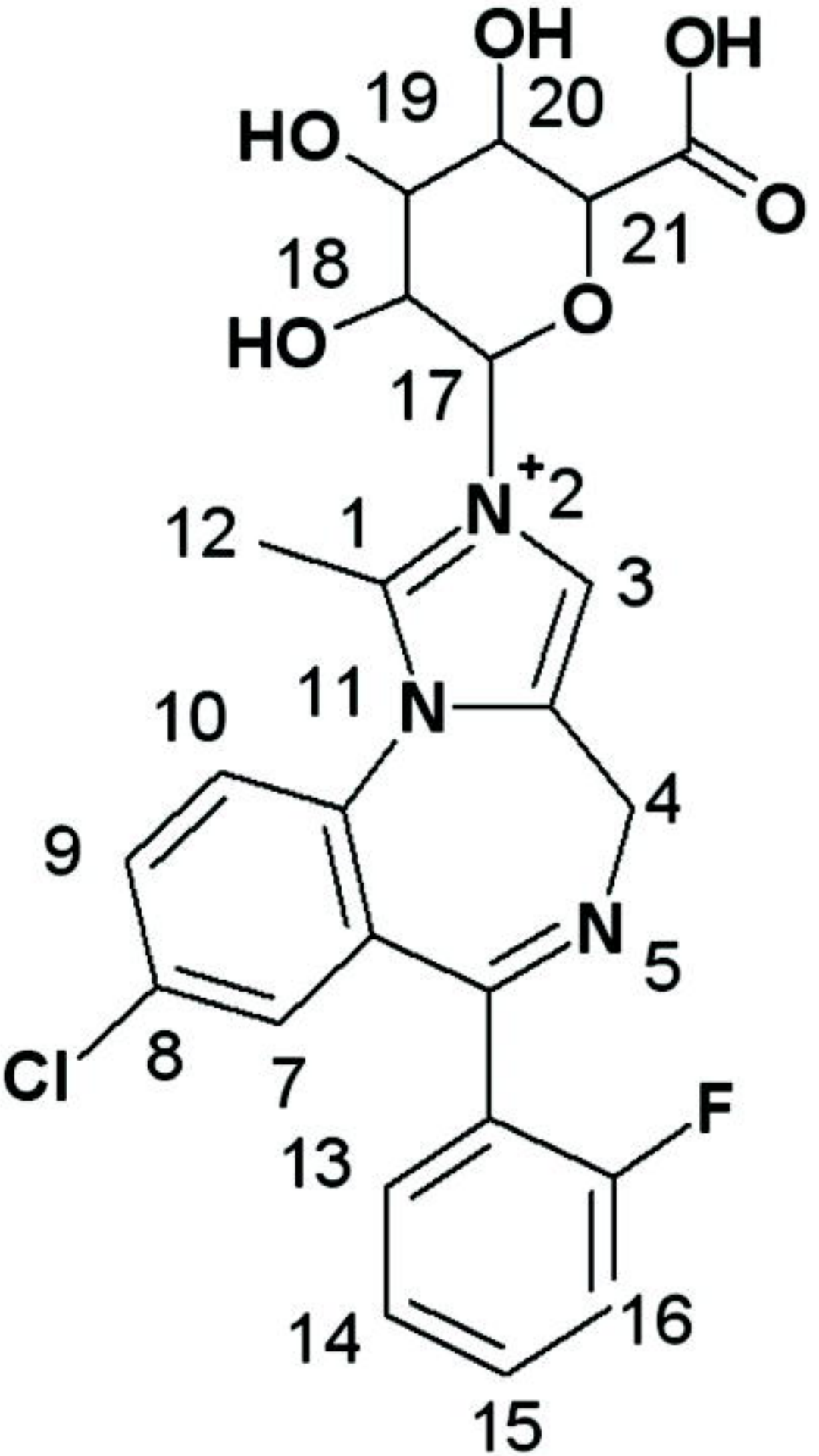

DMD Fast Forward. Published on February 6, 2008 as DOI: 10.1124/dmd.107.019539

Figure 7

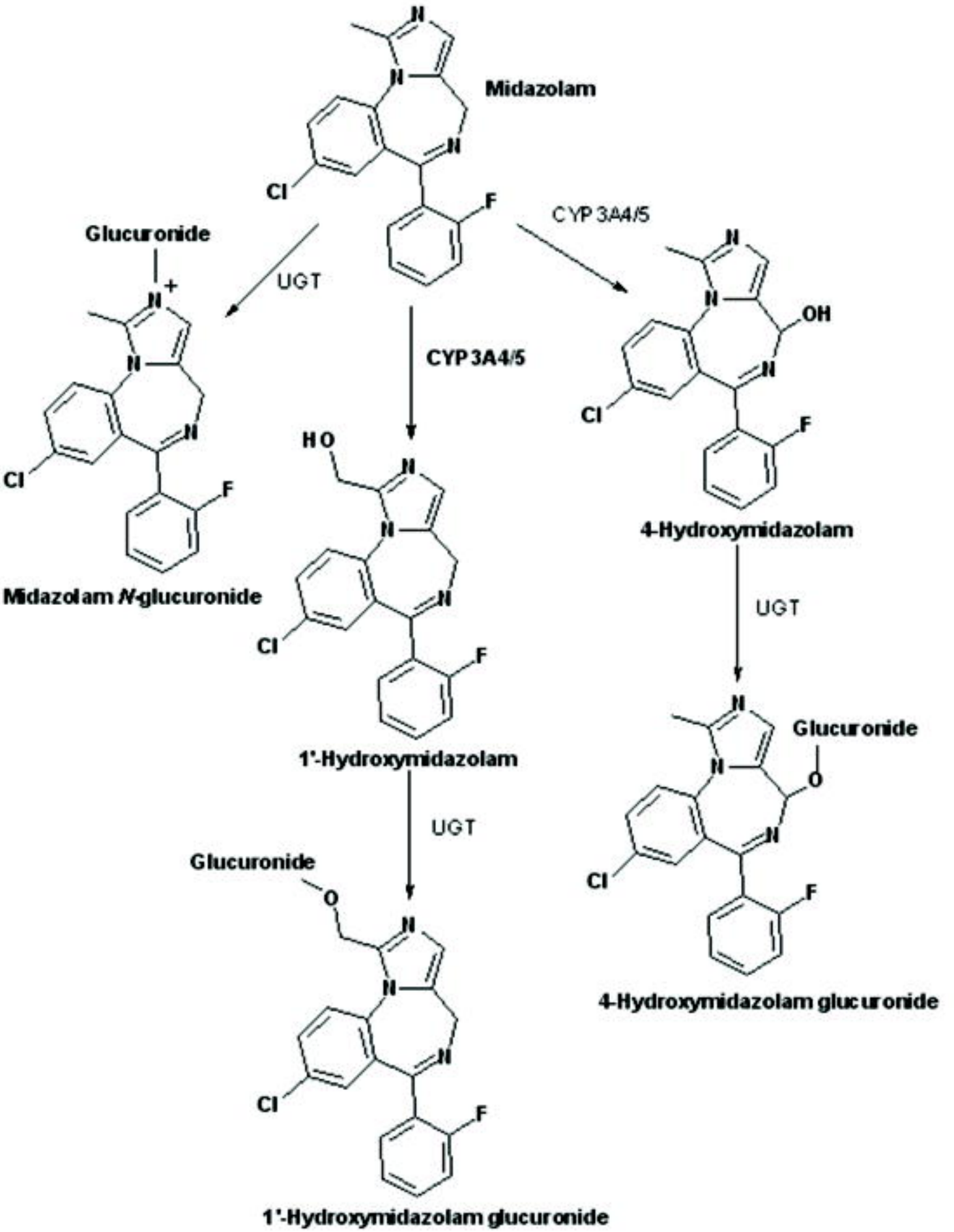

Figure 8

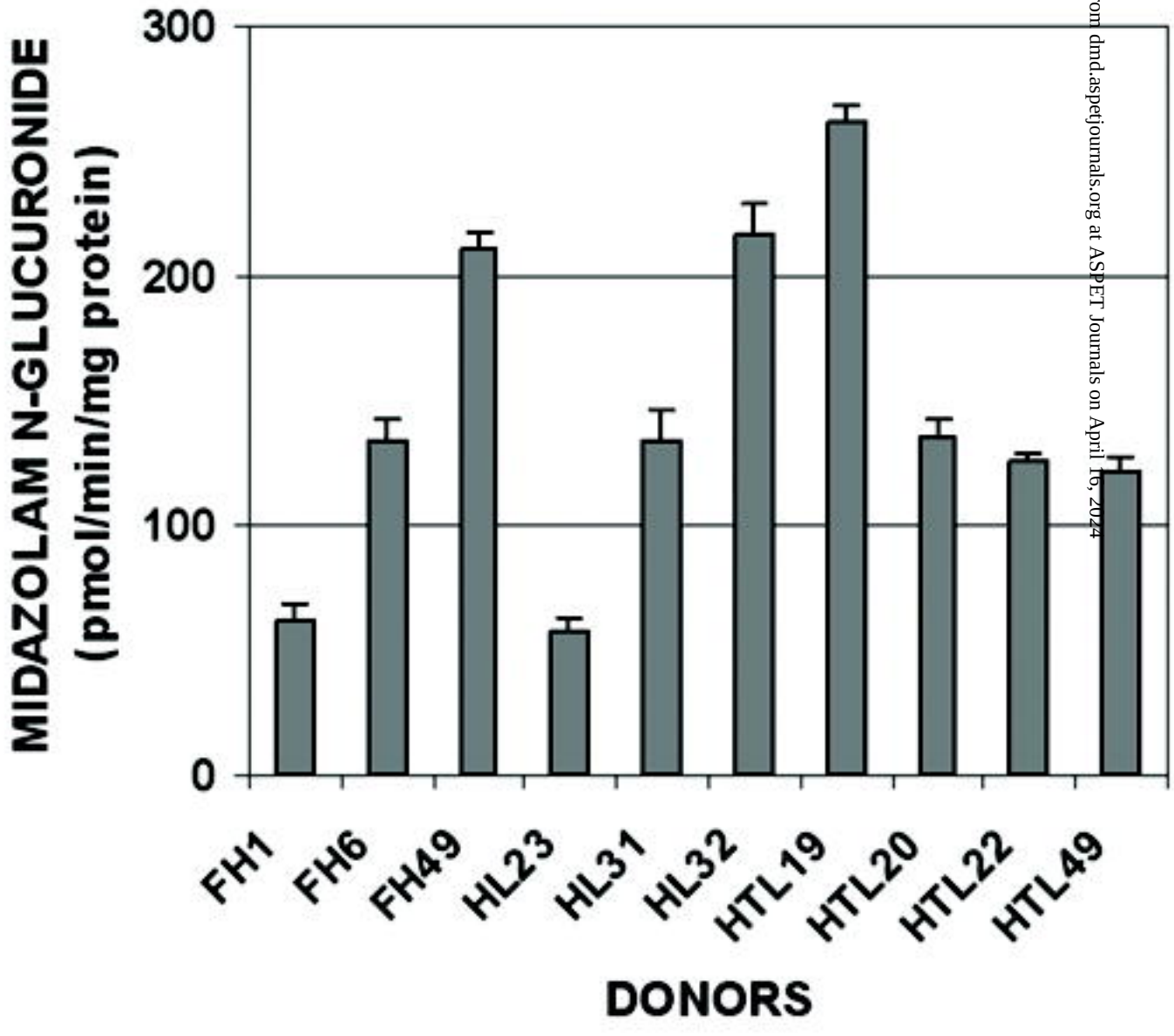

Figure 9

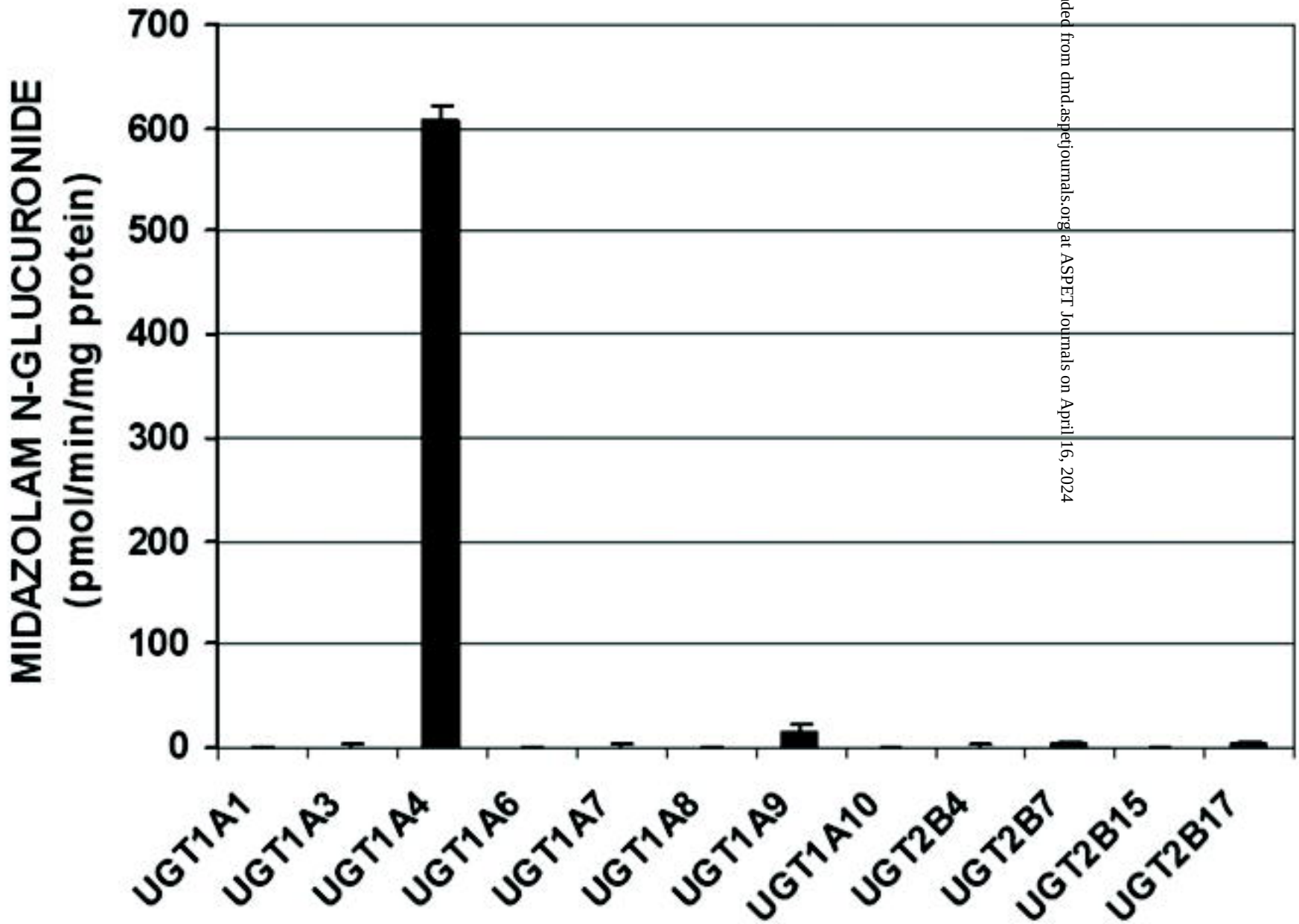

DMD Fast Forward. Published on February 6, 2008 as DOI: 10.1124/dmd.107.019539

Figure 10

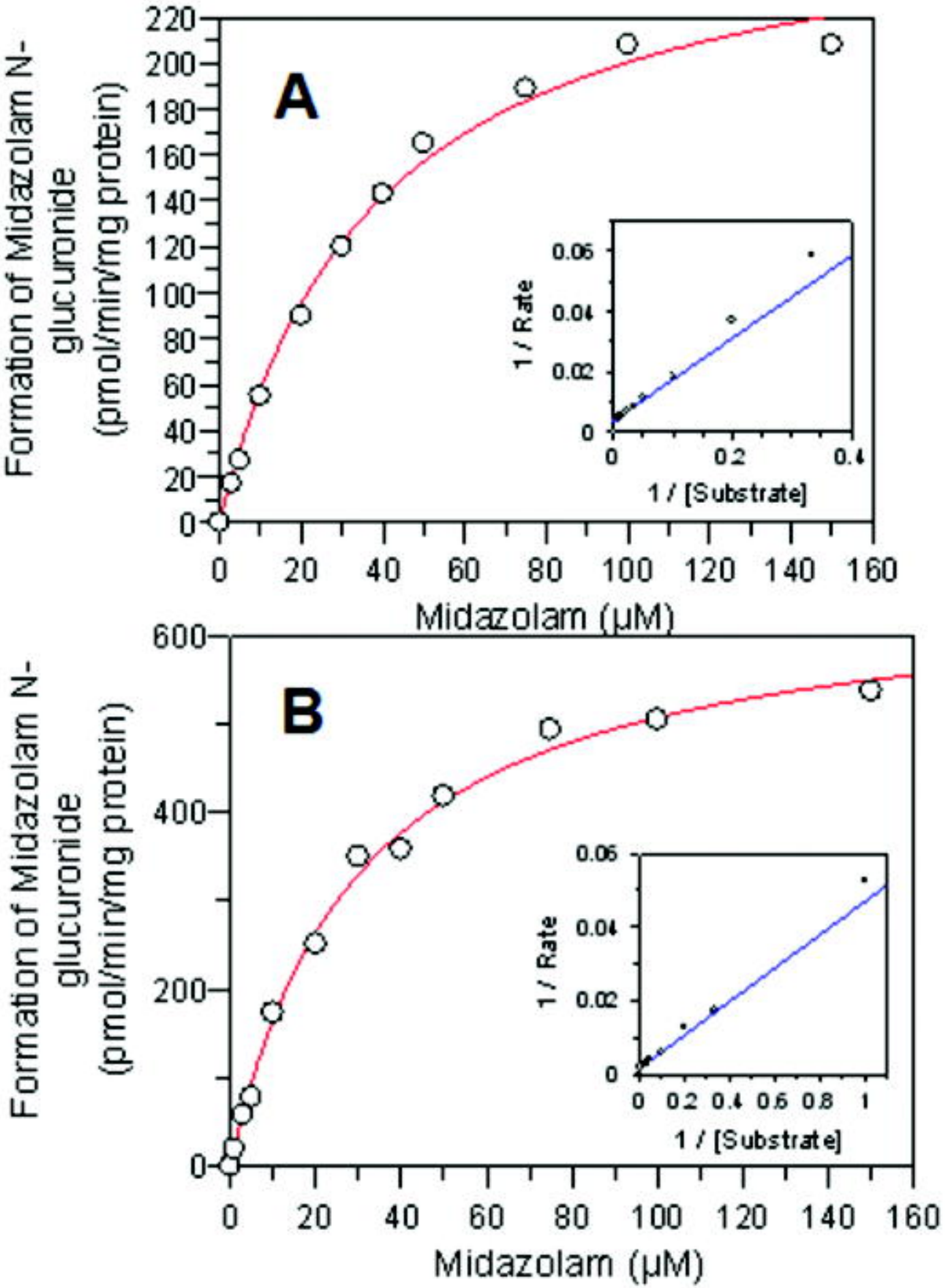

Figure 11

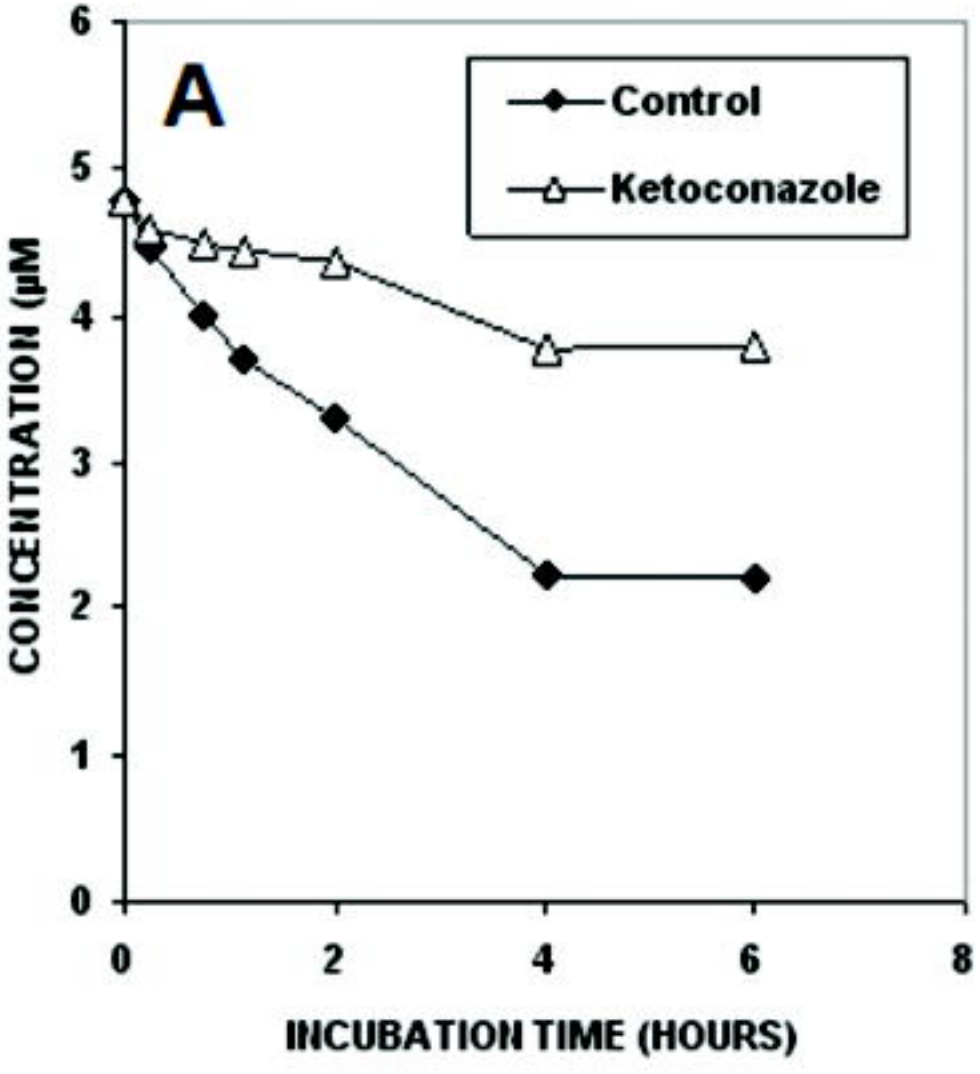

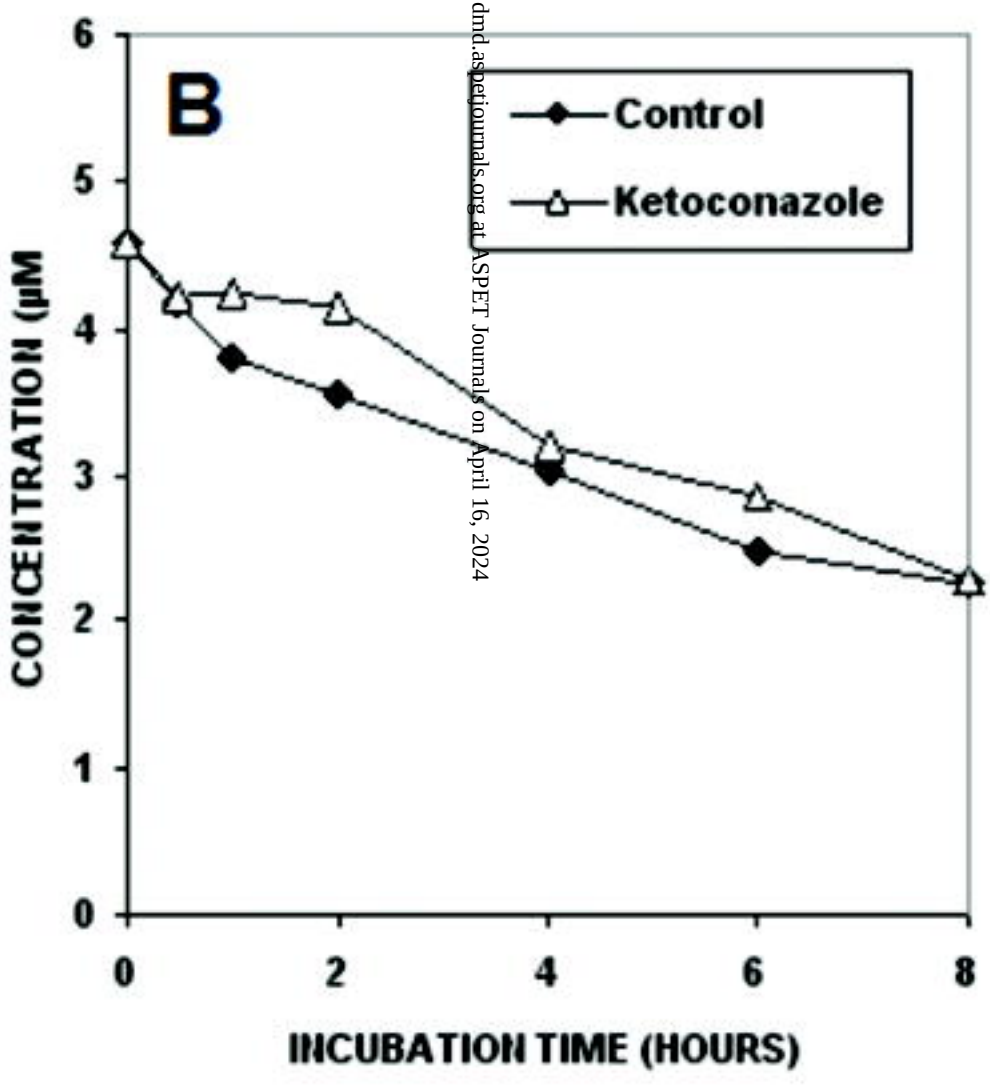

Figure 12

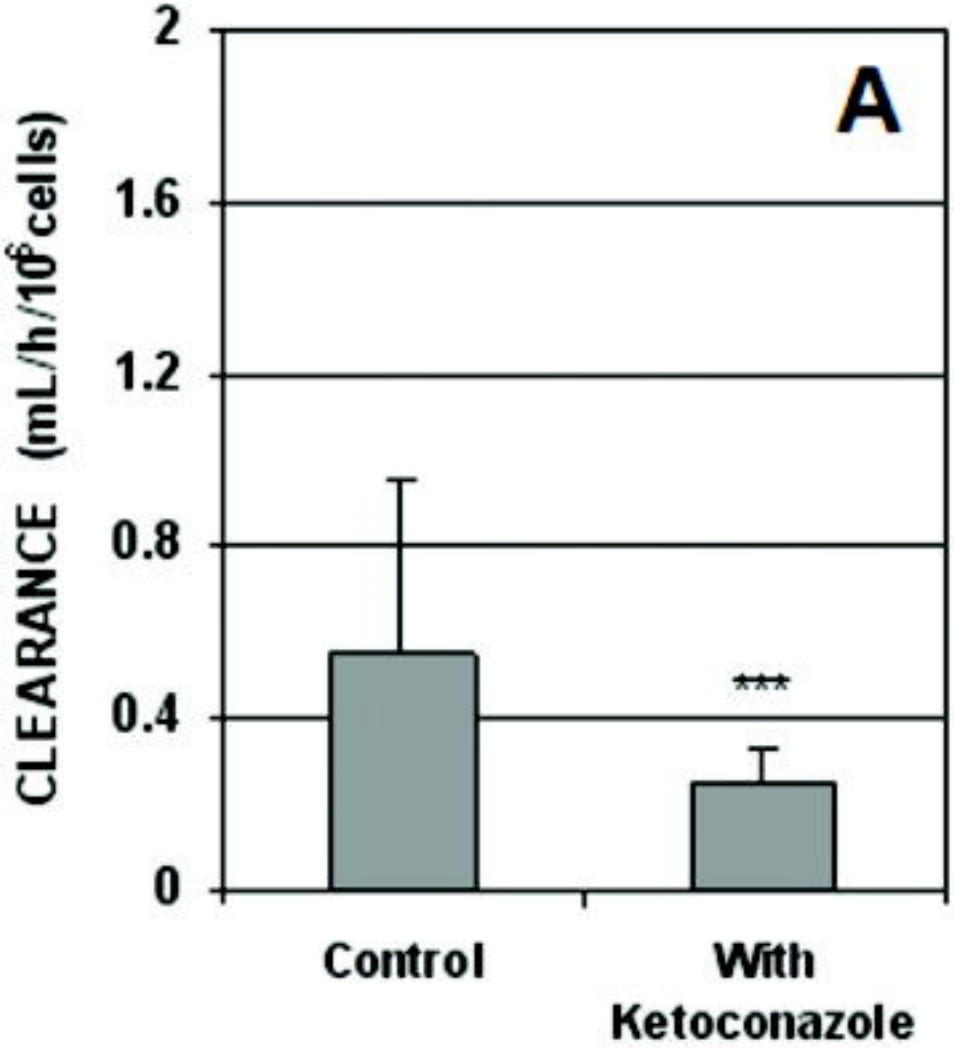

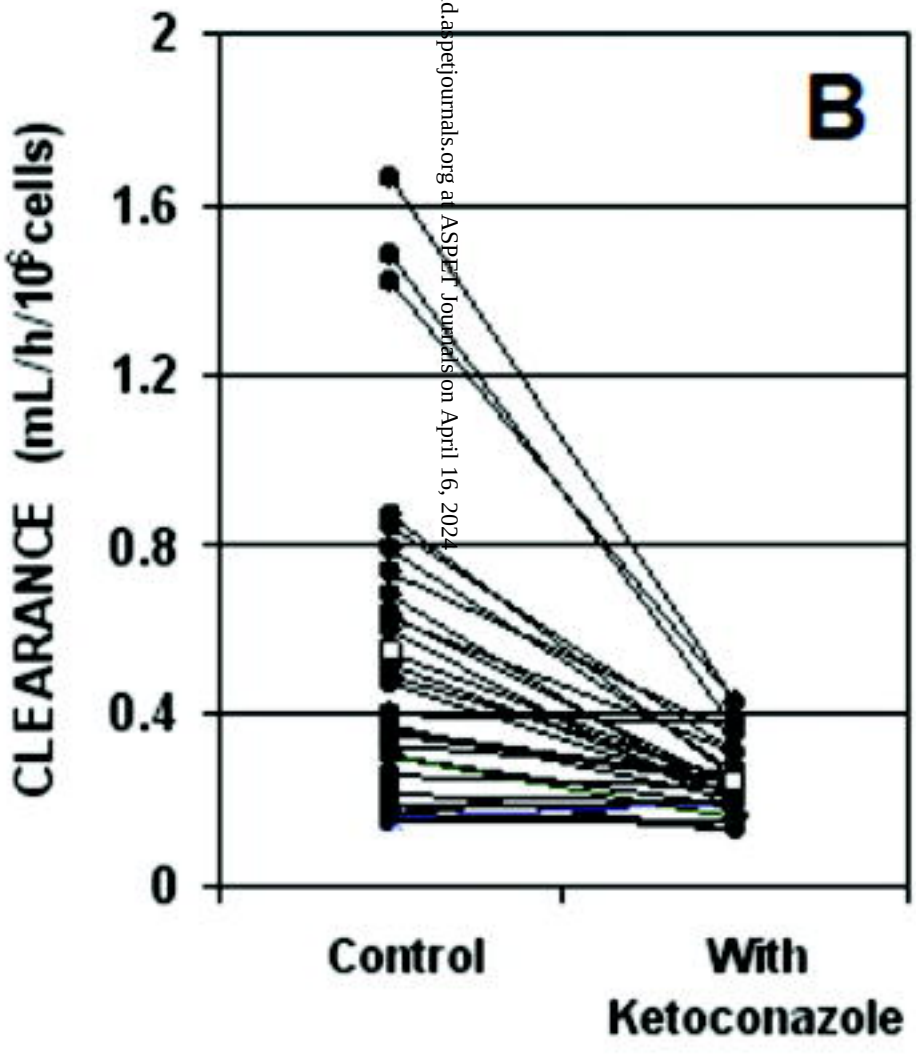

DMD Fast Forward. Published on February 6, 2008 as DOI: 10.1124/dmd.107.019539
This article has not been copyedited and formatted. The final version may differ from this version.

Figure 13

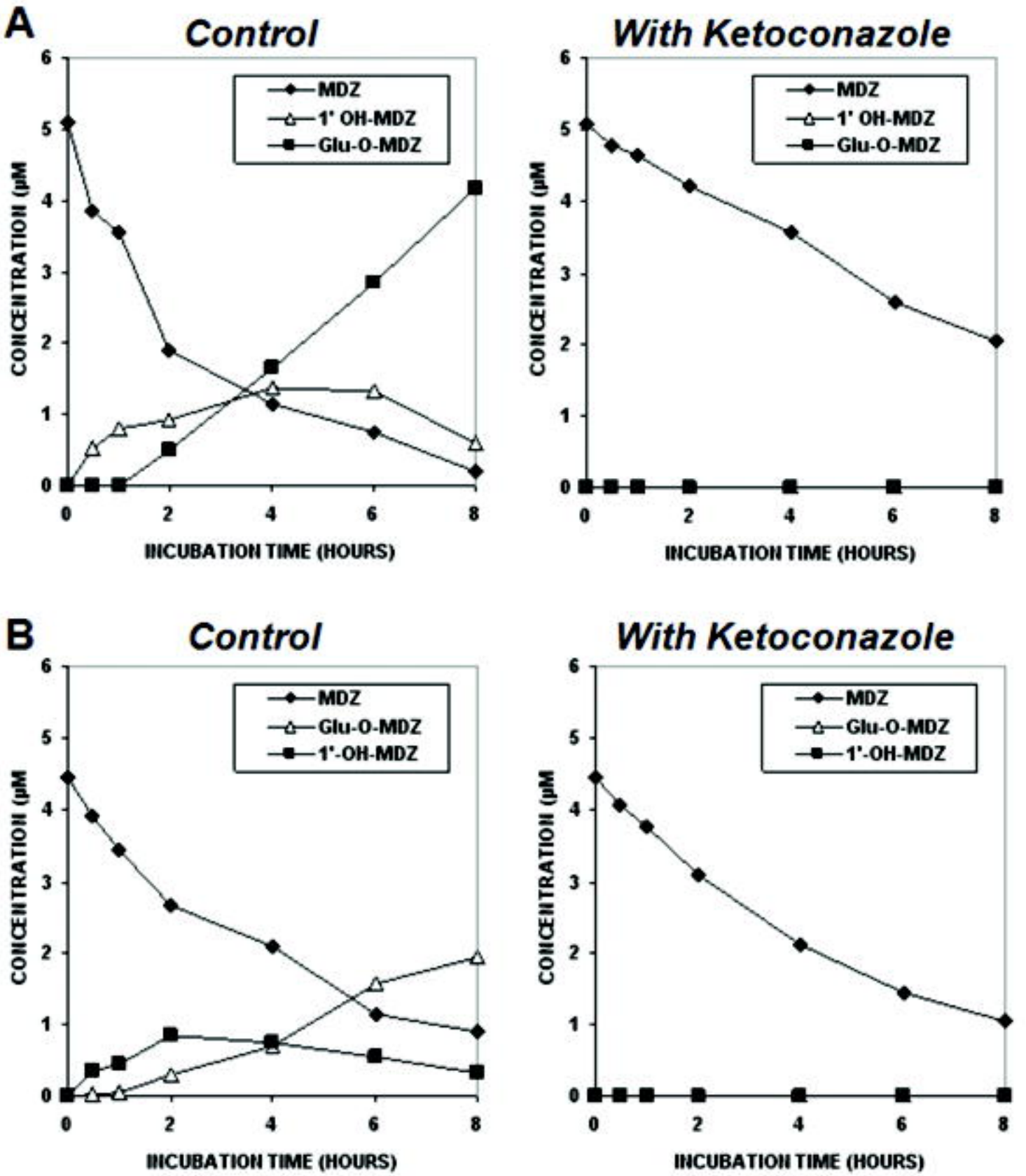

Figure 14

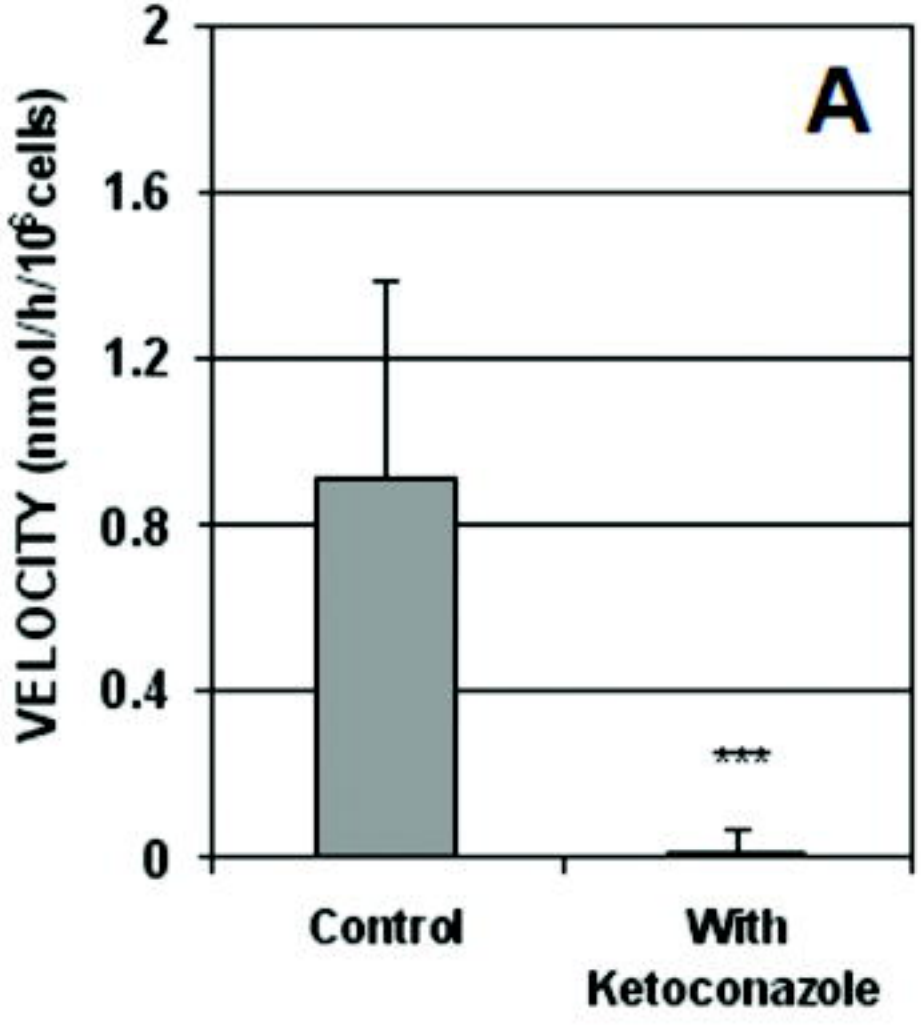

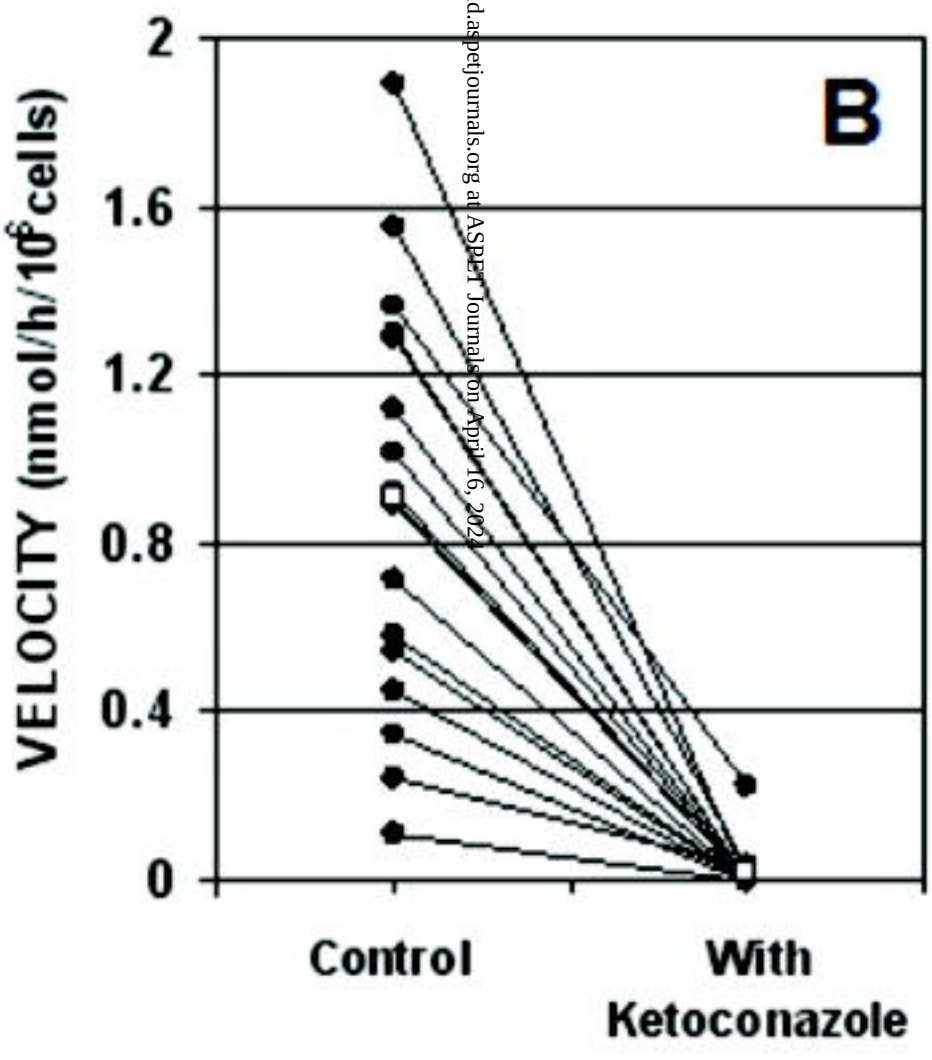

DMD Fast Forward. Published on February 6, 2008 as DOI: 10.1124/dmd.107.019539
This article has not been copyedited and formatted. The final version may differ from this version.

Figure 15

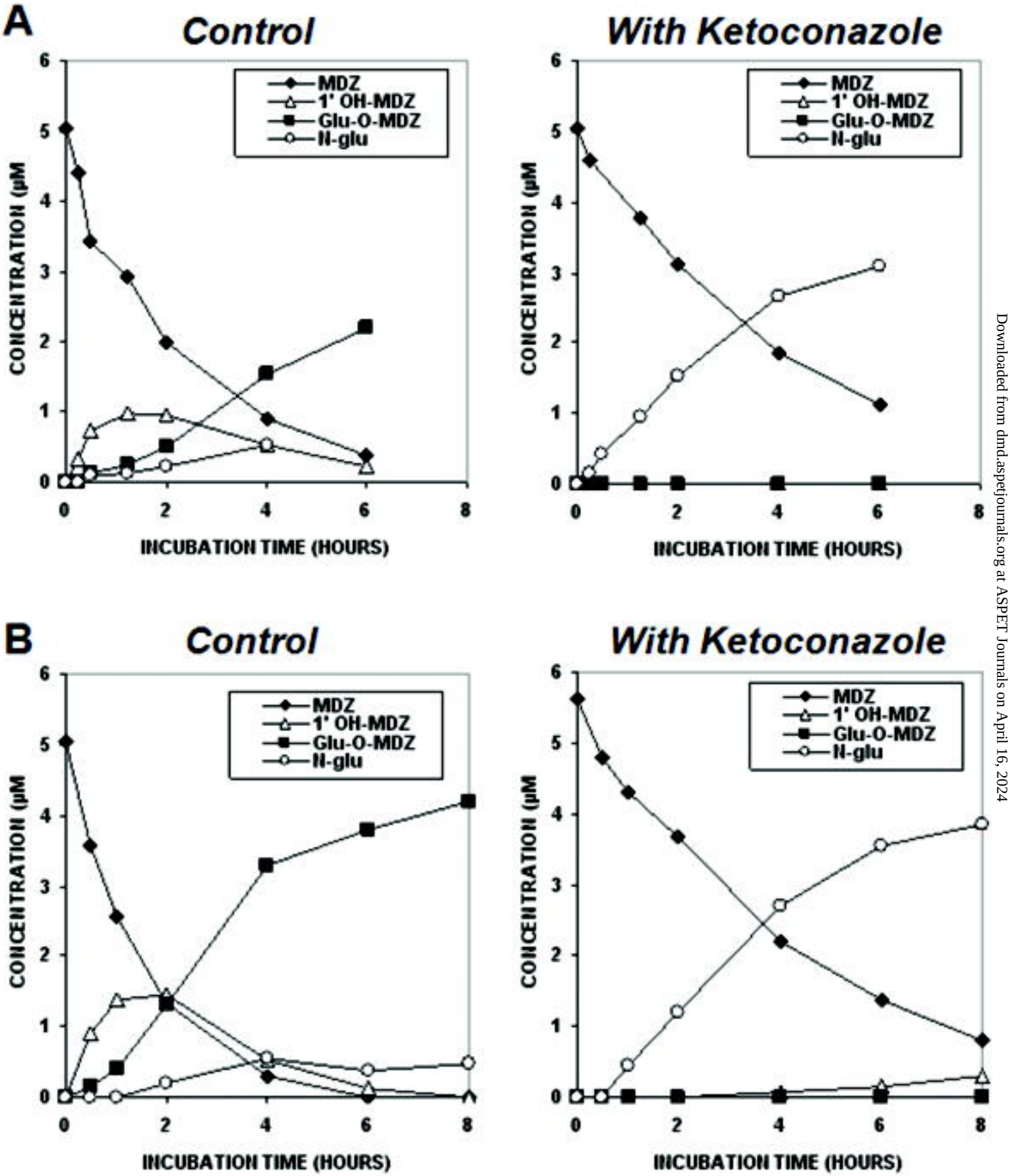

Figure 16